Muon Trigger Documentation

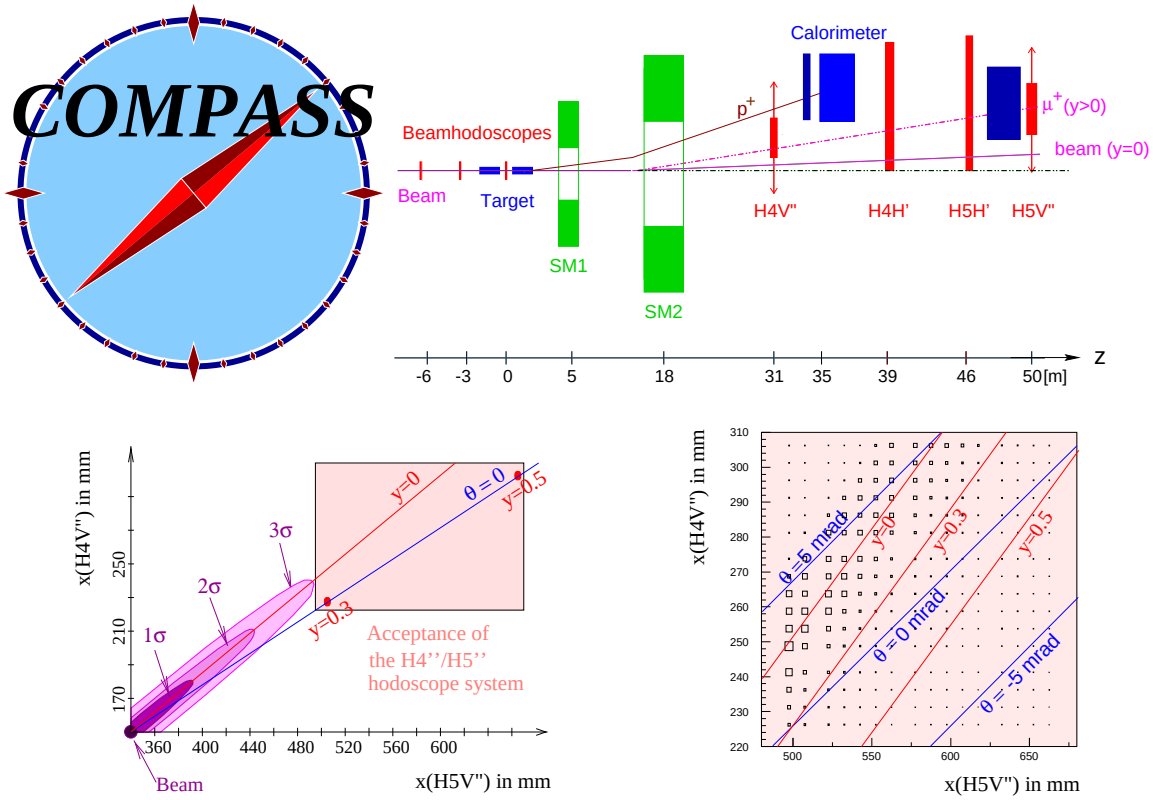

The muon trigger group

June 3, 2002

This document contains a description of the aims and methods, devices and procedures of the muon trigger for the COMPASS experiment.

Contents

1 Introduction

The muon trigger system selects certain classes of muon scattering events with the help of dedicated trigger hodoscopes and the standard hadron calorimeters HCAL1 and HCAL2. The selection is based on the geometric properties of the track of the muon candidate and on the energy deposition in the hadron calorimeters which are shielded from the electro-magnetic quanta by either ECAL1 and ECAL2 or lead walls of about 10 cm thickness ($\approx$18 X_0). The trigger has to provide the start of the data aquisition (CATCH boards) and is used for the readout of specific equipment types which need an external timing signal like the ADC readouts of the calorimeters and the RICH detectors.

The general design of the trigger system is aimed at a high selectivity and a high efficiency for the selected event classes. The number of usable triggers is limited by the speed of the transfer to the central data aquisition system of about 30 Mbyte/s. Without further selection due to a second level trigger this corresponds to about 20 000 events per spill. An exact event timing is needed to attach in a unique way an incoming and outgoing muon track candidate to the event.

The trigger should be able to select two very different event classes:

1. The quasi-real photon events with small four momentum transfer ($Q^2 < 1\,\mathrm{GeV}^2$) and photon energies above a selected cut value of typical $\nu_{min} = 0.3 \times E_{beam}$. This event class *requires* a hadron calorimeter signal to reject (i) radiative and (ii) $\mu\,e$ scattering events in the target as well as (iii) low energy halo tracks.

2. Inclusive deep inelastic scattering events with $Q^2 > 1\,\mathrm{GeV}^2$ covering the full x-range. The acceptance is typically limited by the window size of the spectrometer magnet SM2 of $1 \times 2\,\mathrm{m}^2$ at about 20 meter distance from the target. At a beam energy of 200(190) GeV this limits the four momentum transfer to about $Q^2 \approx 80\,\mathrm{GeV}^2$ at x=1 and $Q^2 \approx 28\,\mathrm{GeV}^2$ at x=0.1.

The hodoscope system is subdivided into a number of multi element modules with different sizes and positions along the beam axis to take care of the very uneven rate distribution and resolution requirements. Figure 1 shows the overview of the experiment with the position of the trigger hodoscopes and the calorimeters.

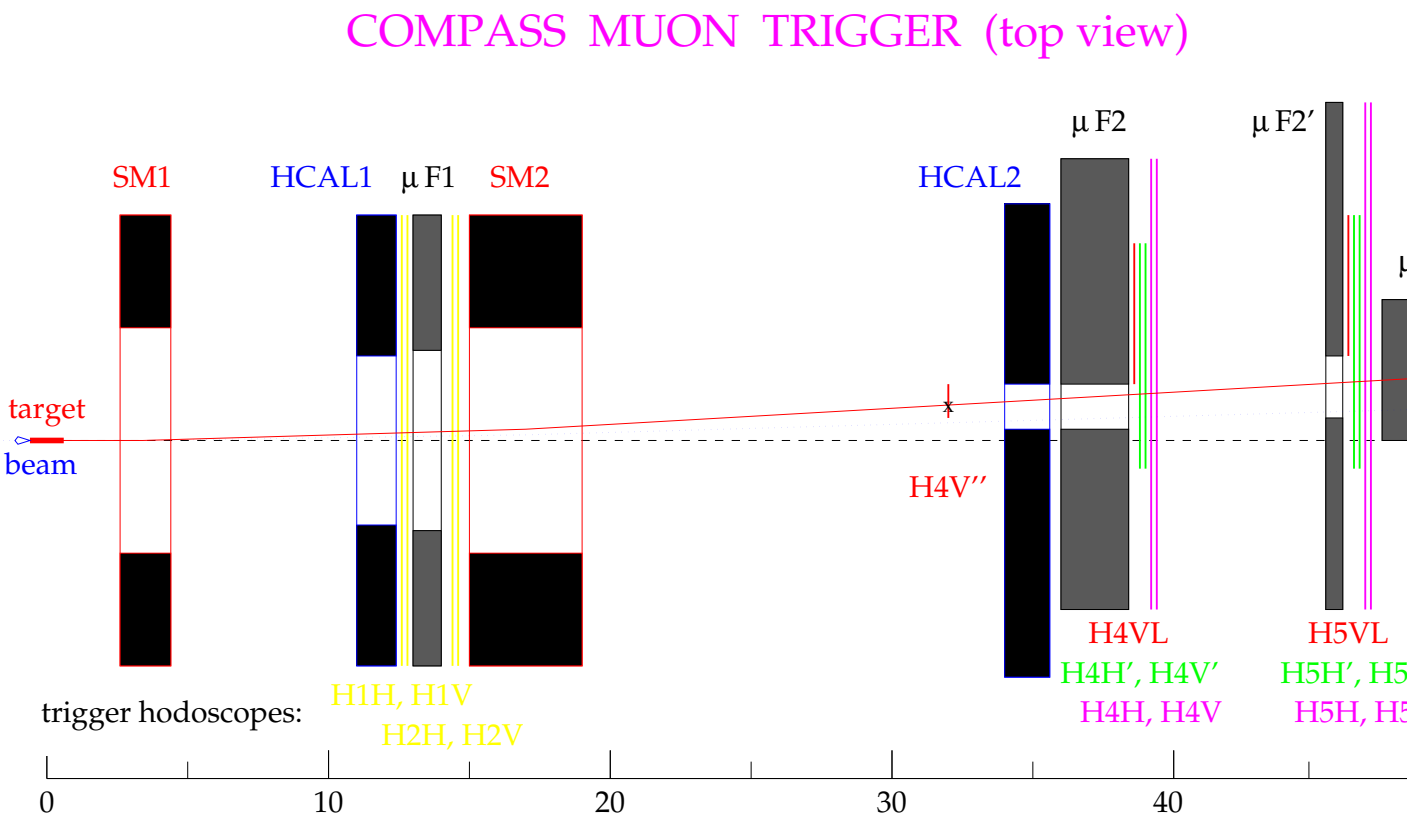

Δ G: (H4V′′ * H5V′′) * (HCAL1 U HCAL2) (low v)

(H4VL * H5VL) * (HCAL1 U HCAL2) (high v)

Figure 1: Overview

2 The Trigger Concept

As pointed out in the Introduction there are two very different event classes to be selected with very different resolution and background conditions.

2.1 Quasireal Photon Trigger

2.1.1 Properties of quasireal photoabsorption events

As described in the COMPASS proposal the measurement of the gluon polarisation is based on the measurement of the double polarized asymmetries of certain semiinclusive cross sections at low or even minimum four momentum transfer (μ-scattering angle ≈ 0) which involve at least two (medium) high transverse momentum hadrons. The photon energy has to provide sufficient invariant energy in the photon-gluon subsystem to allow a perturbative treatment. We consider $s \approx 10\,\mathrm{GeV}^2$ as sufficiently high. The energy of the photon gluon subsystem is given by $s = x_G \cdot 2M \cdot \nu$. At low $\nu \approx 30(60)\,\mathrm{GeV}$ this allows to sample gluons at $x_G > 0.16(0.08)$. A minimum relative energy loss of $y = \frac{\nu}{E_{beam}} > 0.3$ is needed to provide a sufficient photon polarisation. An event with a sufficient invariant energy of the subsystem will manifest itself by either the production of heavy quarks (charm) or by a pair of high transverse momentum hadrons with $p_\perp > 1.5\,GeV$.

In the following we will discuss experiments at two different beam energies 100 GeV and 200(190) GeV. A basic idea was to have a scalable trigger setup which allows running at all intermediate beam energies. The cuts will be set at $y > 0.3$. The minimum four momentum at zero scattering angle transfer is given by $Q^2_{min} = \frac{m_\mu^2 \cdot \nu^2}{E_{beam}(E_{beam}-\nu)}$. In order to have a reasonable coverage of the cross-section as a function of $Q^2 > Q^2_{min}$ the acceptance should be extended to 5 mrad. This corresponds to 90% of the quasireal cross section at $\nu = 30(60)$GeV.

The cross section as a function of ν increases like $1/\nu$ towards small ν. The cross section in the interval $0.1 < y < 0.3$ corresponds to about x times of that in the relevant interval $0.3 < y < 1$.

In principle ν could be measured calorimetrically only. In the trigger radiative processes and $\mu\,e$ scattering events have to be suppressed. This can be achieved by requiring a minimum hadronic energy. Since part of the hadronic energy appears as $\pi^0 \to 2\gamma$ which is not seen in the hadron calorimeter the trigger threshold has to be set as low as possible to account for extreme fluctuations.

Another source of fluctuations are the inevitable deviations of the calorimeters from the ideal full containment. There are holes and cracks and calibration problems due to the combination of HCAL1 and HCAL2. In addition semileptonic decays may lead to a systematic underestimation of the hadronic energy. The lowest possible threshold in the calorimeters is defined by the response of the numerous halo muons which typically deposit an equivalent of 1 mips=2 GeV in the hadron calorimeter. If the calorimeters do not have an ideal spatial independence of the response to muons the effective threshold will increase, since it has to take care of the cases with the highest response.

At the very small scattering angles of quasireal photonabsorption events the accuracy of the track measurements of the incoming and outgoing muons will not allow to determine a longitudinal vertex position with a precision which would allow to separate events stemming from the two target halves. However, the transverse vertex position can be reconstructed with a mm resolution given by the scintillating fiber detectors in front and behind the target. The true longitudinal vertex position will rather be determined by the hadron tracks with large transverse momentum and a correspondingly high longitudinal resolution. The delayed decay of charmed hadrons occurs within a few mm well within the resulting longitudinal vertex resolution. A detection of several longitudinally separated vertices will hint to Λ or K decays, secondary interactions or multiple events within the experiments time resolution.

For trigger purposes and acceptance calculations the vertex will be assumed to be positioned somewhere in the target cylinders of 3 cm diameter and 2*60 cm length with the 10 cm gap in between.

In the initial trigger setup there will be no beam hodoscope or beam momentum station information used to form the trigger. This option exists and may be used at a later stage to enhance the lateral vertex resolution and to reject events with an incoming track missing the target (near halo) or to assure reconstructability of the muon kinematics.

2.1.2 Geometrical properties of the scattered muon track

The muon beam has a considerable emmitance of about 10 mm mrad with a gaussian core plus exponential tails (see fig. 30). In addition the beam has a chromaticity of about 5% sigma. The magnet configuration of SM1 and SM2 (see fig. 1) serves to separate tracks with a relative energy loss of larger than y=0.3 from the

volume occupied by the deflected noninteracting beam so that the trigger devices can be positioned outside the (deflected) beam core. As discussed in the previous section the trigger has to deal with muons with scattering angles from 0 to 5 mrad. A simple measurement of the x-coordinate (in the bending plane) of the outgoing muon relative to undeflected beam line will not be sufficient to determine the relative energy loss y. The combined measurement of the x-coordinate at two different z-positions (along the undeflected beam direction) can disentangle the magnetic deflection $\beta = \frac{0.3 \cdot \int B\, dl}{p'_\mu} = \beta_0 \cdot \frac{p_{beam}}{p'_\mu} = \beta_0 \frac{1}{1-y}$and the horizontal component of the scattering angle θ_x. The choice of the magnet configuration determines β_0 which is the beam deflection angle and the so called pivotal point z_m which determines the position of the bending center along the beam(z) direction. The target center is at $z = 0$. For the trigger discussion we utilize a simplified description of the magnetic fields. We use the approximation of two kicks at the position of the center of SM1 at $z_{SM1} = 3.5$ m and of the center of SM2 at $z_{SM2} = 17.3$ m. The pivotal point is positioned at $z_m = \frac{z_{SM1} \cdot \int B_1 dl + z_{SM2} \cdot \int B_2 dl}{\int B_1 dl + \int B_2 dl}$. In a previous trigger note (Oct. 2 1998 appendix 1) we have discussed different configurations. In order to provide an essentially scalable setup (for different beam energies) and in order have a maximum separation of the scattered muon from the beam we use parallel fields in SM1 and SM2 which provide a combined deflection of $\beta_0 = 10$ mrad and a pivotal position of $z_m = 13.11\,\mathrm{m}$ (100 GeV) and $z_m = 15.07\,\mathrm{m}$ (190 GeV).

Two hodoscopes, H4VIand H5VI, will be positioned at $z_1 = z_{\mathrm{H4VI}} = 32.0$ m and $z_2 = z_{\mathrm{H5VI}} = 51$ m to measure the x coordinate of the track.For x_1 and x_2 we get:

$$\begin{aligned} x_1 &= x_0 + \theta_x \cdot z_1 + \beta_0 \cdot \frac{p_0}{p'}(z_1 - z_m) \\ x_2 &= x_0 + \theta_x \cdot z_2 + \beta_0 \cdot \frac{p_0}{p'}(z_2 - z_m) \end{aligned} \tag{1}$$

The values of the scattered muon parameters x_0, θ_x and p' are the same. Multiple scattering is not taken into account. The unknown horizontal component of the scattering angle can be eliminated from the equations and one arrives at:

$$\frac{x_1 \cdot z_2 - x_2 \cdot z_1}{z_2 - z_1} = x_0 - \beta_0 \cdot \frac{p_0}{p'} z_m \tag{2}$$

The expression on the left hand side measures the scattered muon energy p' up to the unknown horizontal vertex position x_0 (for a thin target). Without using the information from the beam hodoscope in the trigger this parameter has to be treated as an error of about $\sigma_{x_0} = 8.6$ mm. p_0 is the nominal average beam momentum. The error on p' is given by the errors from the measurements of x_1 and x_2 and the error on the vertex position. There is no dependence on the incoming muons energy or angle of incidence. There is however an uncertainty induced on the determination of the relative energy loss y and the scattering angle θ_x.

The correlation of $x_1 = x_{\mathrm{H4VI}}$ and $x_2 = x_{\mathrm{H5VI}}$

$$x_1 = \frac{z_1}{z_2} \cdot x_2 + \frac{z_2 - z_1}{z_2}(x_0 - z_m \beta_0 \frac{p_0}{p'}) \tag{3}$$

is illustrated in fig. 37.

The lines of constant scattered momentum have a constant slope $\frac{dx_1}{dx_2} = \frac{z_1}{z_2} \approx 0.62$ which is entirely determined by the choice of the hodoscope positions z_1 and z_2 . Alternatively one can also eliminate p' from the equations (1) and arrives at

$$x_1 = \frac{z_1 - z_m}{z_2 - z_m} \cdot x_2 + \frac{z_2 - z_1}{z_2 - z_m}(x_0 + z_m \cdot \theta_x) \tag{4}$$

The lines of constant (horizontal)scattering θ_x have a different slope of $\frac{dx_1}{dx_2} = \frac{z_1 - z_m}{z_2 - z_m} \approx 0.46$ which again is determined by the position of the hodoscopes and the bending center (pivotal point) of the magnet system z_m.

2.1.3 Triggersignals for quasireal photon events

The muons corresponding to quasireal photon events cover a region concentrated in the bending plane on the Jura side of the spectrometer. For the minimum energy losses to be triggered on, the angle the magnetic deflection angle is comparable to the scattering angle. A sharp energy cut, which is necessary to remove the abundant small energy loss events from the trigger candidates, is only possible if the two effects can be separated. The gain in doing so is the suppression of the events which are above threshold in the calorimeters but below the physics cut in y.

The energy cut independent of the horizontal component of the scattering angle (including multiple scattering in the target and the divergence of the beam) is made in the correlation matrix of the two finely segmented hodoscopes H4VIat z=32m and H5VIat z=51m which cover the near beam region with vertical elements. For rate and time resolution reasons the hodoscopes are separated in an upper and lower half with single ended readout. The element length are then typically 15-30 cm. The scheme of the trigger is illustrated in fig. 2.

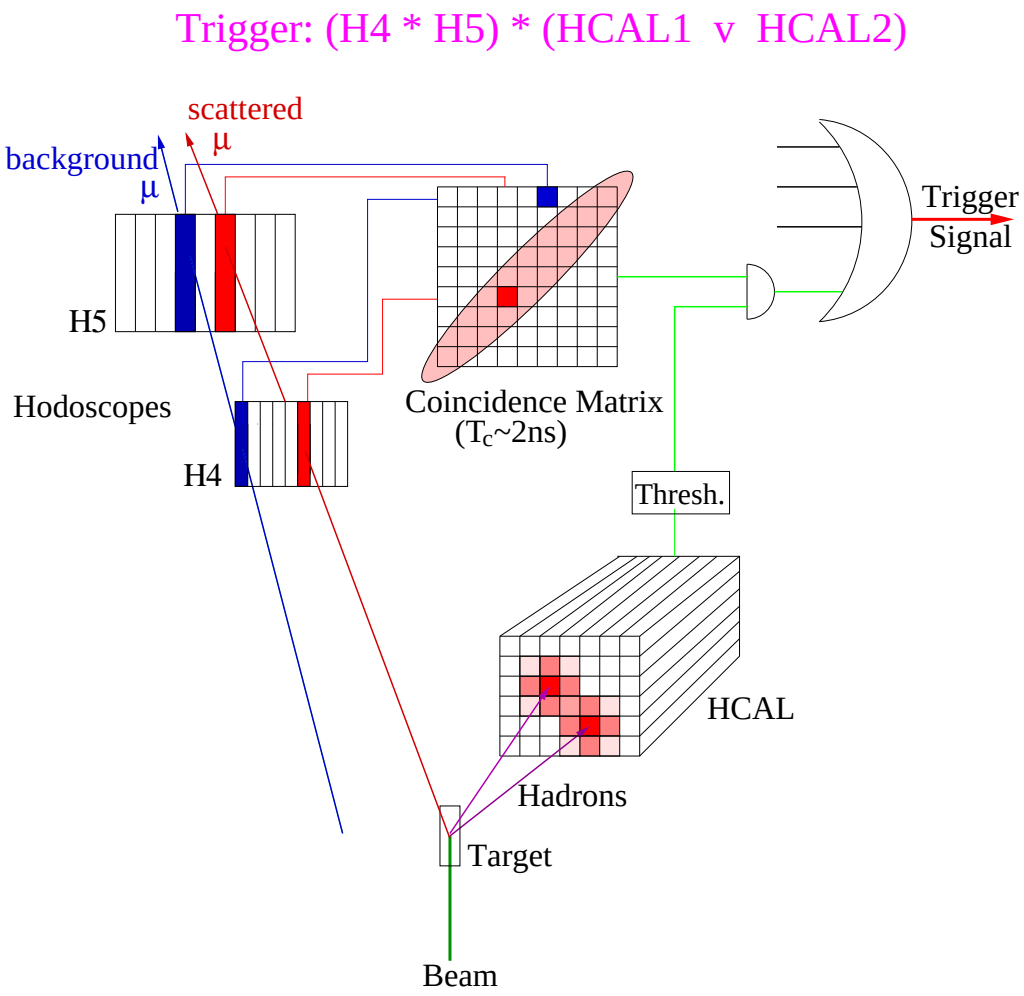

Figure 2: The quasireal photon trigger

The sharpness of the cut on E', which corresponds to a y- or ν-cut only if the incoming muon energy has a sharp value, depends on the width of the hodoscope elements and the size of the target if there is no multiple scattering for the outgoing muon. We therefore require that the muons in the region where the cut has to be performed does not pass through absorbers. The only absorber allowed is just in front of the H5VIwhere multiple scattering is not effective to spoil the position information. This iron absorber of 1.5m serves as a filter for hadrons, photons and electrons.

3 The Trigger Hodoscopes

This chapter contains the details (sizes, positions etc.) about the trigger hodoscopes foreseen for the initial setup. The numbers are calculated for a beam energy of 190 GeV, 1 Tm in SM1 and 5.2 Tm in SM2.

3.1 The Inner System[1] (ΔG, low ν)

The inner system consists of two hodoscope planes with vertical scintillator strips. As described in sec. 2.1 it covers the low ν part for events with scattering angles below 5 mrad.

H4VIis located in front of ECAL2 at 32 m, H5VIbehind the last iron absorber (MF3) at 51 m. Figure 3 shows the schematic layout of the inner hodoscopes.

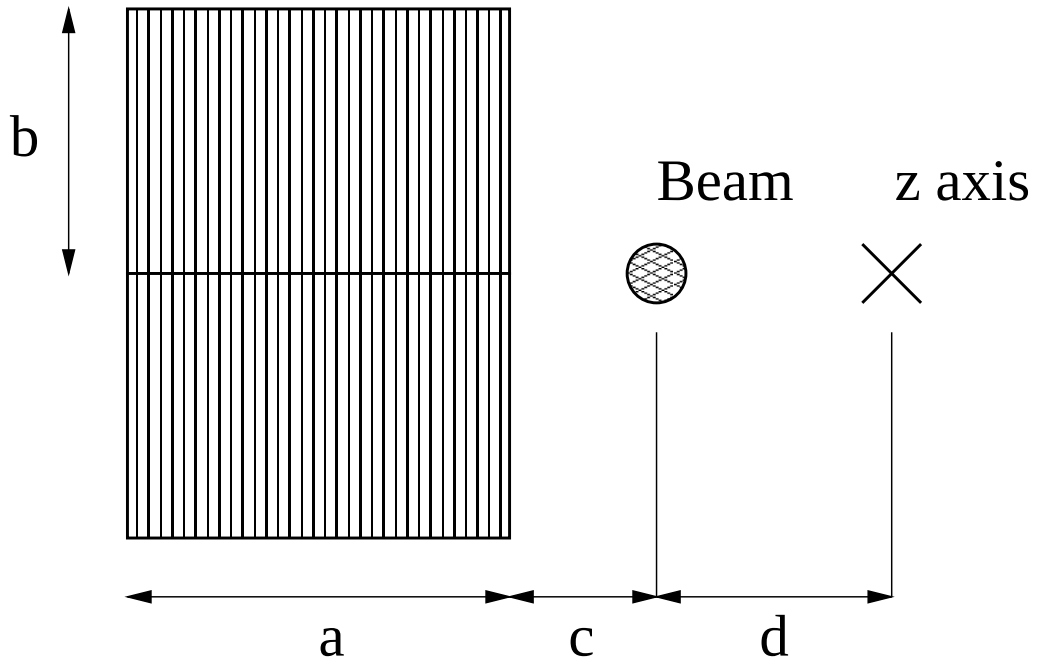

Figure 3: Scheme of the Inner Hodoscopes.

Each hodoscope is split in an upper and a lower part. The scintillators are read out by PM's via lightguides on one side. H4VIis inclined by 30 ° to compensate for different length of H5VI.

3.1.1 H4VI

- Position: 32 m.
- Two parts (upper and lower), each with 32 vertical elements.
- Single sided readout
- Element size (width x depth x length): 6x10x194 mm^3 (inclined).
- Overlap: 0.6 mm.
- Hodoscope dimensions (c.f. fig. 3):

Dimension	a	b	c	d
Size [mm]	173.4	160	53	166

- Tubes: R7400.
- Reserved depth: 500 mm
- inclination angle: 30 °.

[1] former: Double Prime System

3.1.2 H5VI

- Position: 51 m.
- Two parts (upper and lower), each with 32 vertical elements.
- Single sided readout.
- Element size (width x depth x lenght): 12x20x259.5 mm^3.
- Overlap: 1 mm.
- Hodoscope dimensions (c.f. figure 3):

Dimension	a	b	c	d
Size [mm]	353	255	124	351

- Tubes: XP2900.
- Reserved depth: 500 mm.

3.2 The Ladders (ΔG, high ν)

The two ladder hodoscopes H4VL and H5VL complement the quasi real photon trigger with the high ν events. They are located behind the muon filters MF2 and MF2P. Their schematic layout is shown in fig. 4.

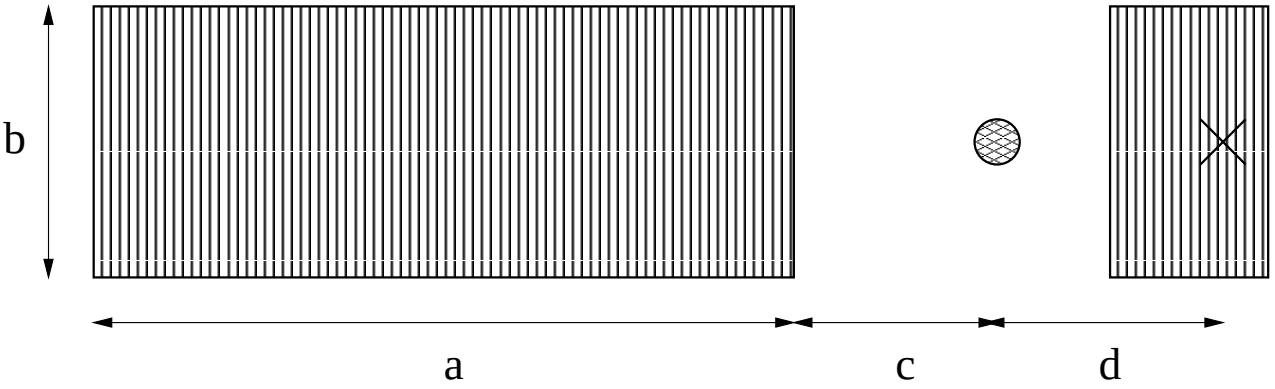

Figure 4: Scheme of the ladder hodoscopes.

3.2.1 H4VL

- Position: 40.564(5) m (measured in November 2001).
- 32 vertical elements.
- Double sided readout.
- Element size (width x depth x lenght):
  - 8 Elements à 22x15x400 mm^3 (XP2900).
  - 8 Elements à 32x15x400 mm^3 (XP2900).
  - 8 Elements à 47x15x400 mm^3 (XP2090).
  - 8 Elements à 67x15x400 mm^3 (XP2020).
- Overlap: 1 mm and 3 mm.
- Hodoscope dimensions (c.f. figure 4):

Dimension	a	b	c	d
Size [mm]	1282	400	295	240

- Tubes: 32 XP2900, 16 XP2090, 16 XP2020.
- Reserved depth: 300 mm.

Remark: An extension on the saleve side of the beam (8 elements) is being considered as indicated in fig. 4.

3.2.2 H5VL

- Position: 48.085(5) m (measured in November 2001).
- 32 vertical elements.
- Doubled sided readout.
- Element size (width x depth x lenght):
  - 8 Elements à 27x15x475 mm^3 (XP2900).
  - 8 Elements à 42x15x475 mm^3 (XP2090).
  - 8 Elements à 62x15x475 mm^3 (XP2020).
  - 8 Elements à 87x15x475 mm^3 (XP2020).
- Overlap: 1 mm and 3 mm.
- Hodoscope dimensions (c.f. figure 4):

Dimension	a	b	c	d
Size [mm]	1682	475	370	300

- Tubes: 16 XP2900, 16 XP2090, 32 XP2020.
- Reserved depth: 30 cm.

Remarks: An extension on the saleve side of the beam (8 elements) is being considered as indicated in fig. 4.

3.3 The Middle System[2] (medium–low Q^2)

The middle system covers the deep inelastic events for scattering angles in the range between 5 and 15 mrad. As described in sec. **??** it consists out of vertical planes, H4VMand H5VM, and horizontal ones, H4HMand H5HMto achieve horizontal and vertical target pointing. H4HM/H4VMwill be positioned behind MF2 and H5HM/H5VMbehind MF2P. The hodoscopes basically extend the inner and ladder system above and below the bending plane, the upper and lower parts are identical. Whereas the horizontal strips are read out via lightguides by PM's on both sides, the vertical strips are only read on one side.

3.3.1 H4HM

- Position: 40.314(5) m (measured in November 2001).
- Two parts (upper and lower) with 16 elements each
- Double sided readout.
- Element size (width x depth x lenght):
  - 16 elements à 21.5x20x1200 mm^3.
  - 16 elements à 25x20x1200 mm^3.
- Overlap: 1 mm
- Hodoscope dimensions (c.f. figure 5):

Dimension	a	b	c	d
Size [mm]	1200	510	240	160

- Tubes: XP2900.
- Reserved depth: 300 mm (together with H4VM).

[2] former: Prime System

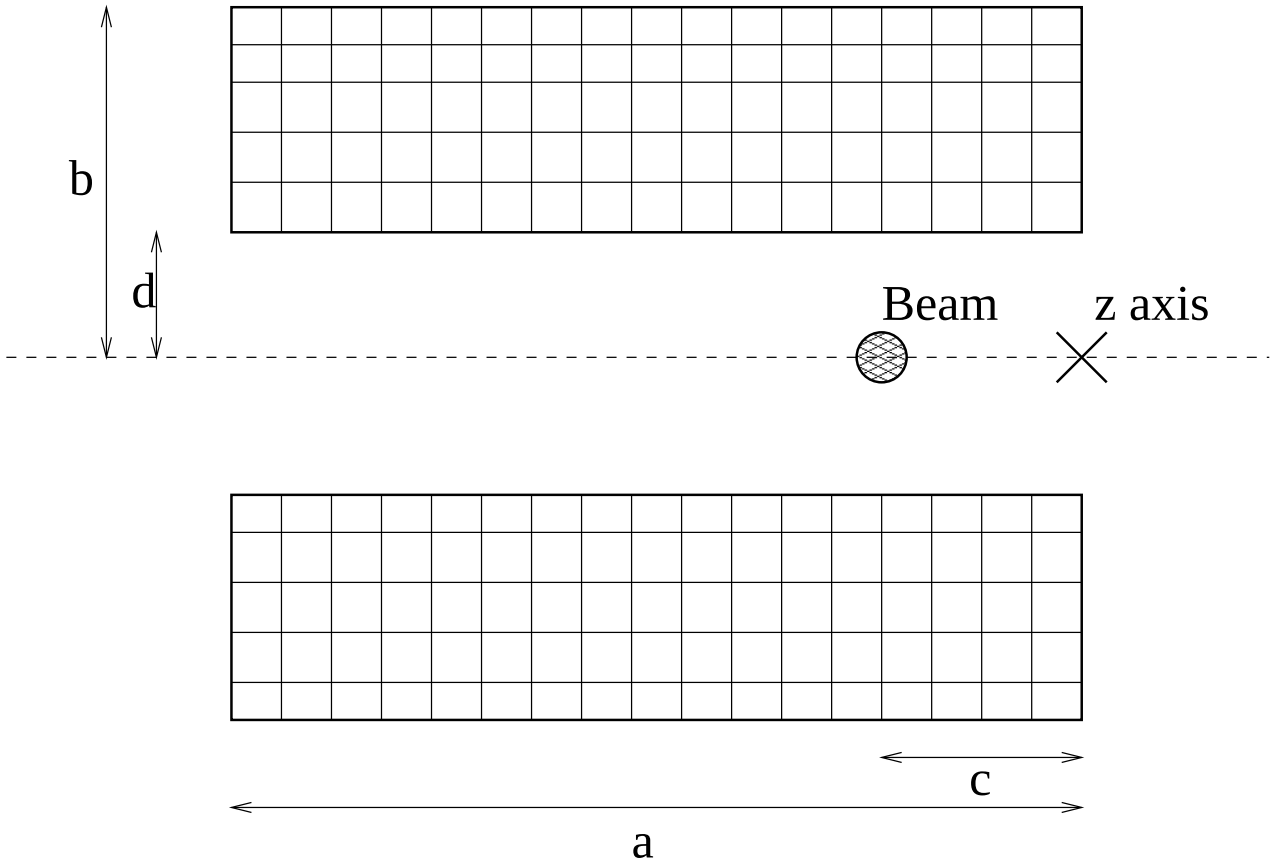

Figure 5: Scheme of the middle hodoscopes.

3.3.2 H4VM

- Position: 40.240(5) m (measured in November 2001).
- Two parts (upper and lower) with 20 vertical elements each.
- Single sided readout.
- Element size (width x depth x lenght): 62x10x355 mm^3.
- Overlap: 1 mm.
- Hodoscope dimensions (c.f. figure 5):

Dimension	a	b	c	d
Size [mm]	1200	510	240	160

- Tubes: XP2072
- Reserved depth: 300 mm (together with H4HM).

3.3.3 H5HM

- Position: 47.844(5) m (measured in November 2001).
- Two parts (upper and lower) with 16 elements each.
- Double sided readout.
- Element size (width x depth x lenght):
  - 16 elements à 25x20x1500 mm^3.
  - 16 elements à 30x20x1500 mm^3.

- Overlap: 1 mm.
- Hodoscope dimensions (c.f. figure 5):

Dimension	a	b	c	d
Size [mm]	1500	600	300	185

- Tubes: XP2900.
- Reserved depth: 300 mm (together with H5VM).

3.3.4 H5VM

- Position: 47.768(5) m (measured in November 2001).
- Two parts (upper and lower) with 20 elements each.
- Single sided readout.
- Element size (width x depth x lenght): 77x10x425 mm^3.
- Overlap: 1 mm.
- Hodoscope dimensions (c.f. figure 5):

Dimension	a	b	c	d
Size [mm]	1500	600	300	185

- Tubes: EMI9954B
- Reserved depth: 300 mm (together with H5HM).

3.4 Summary

	# of Elements	# of MT	# of PMs	Pm Type
H4VI	64	0	64	R7400
H5VI	64	0	64	XP2900
H4VL	32	32	64	XP2900(32)/XP2090(16)/XP2020(16)
H5VL	32	32	64	XP2900(16)/XP2090(16)/XP2020(32)
H4VM	40	0	40	XP2072B
H5VM	40	0	40	EMI9954B
H4HM	32	32	64	XP2900
H5HM	32	32	64	XP2900

Total Number of Scintillator Elements		336
Total Number of Channels		464
Total Number of Meantimers		128
Total Number of Tubes	R7400	64
	EMI9954B	40
	XP2020	48
	XP2072B	40
	XP2090	32
	XP2900	240

3.5 The Outer System[3] (medium–high Q^2)

For the full setup trigger hodoscopes covering the medium and high Q^2 range will be added to the inital setup. The so called outer system will consist of two stations (see fig. 7), one behind SM2 and one behind MF2 each with a horizontal (H3OH/H4OH) plane. The final sizes and positions will also depend on the available large angle tracking system.

[3] former: Unprimed System

3.5.1 H3

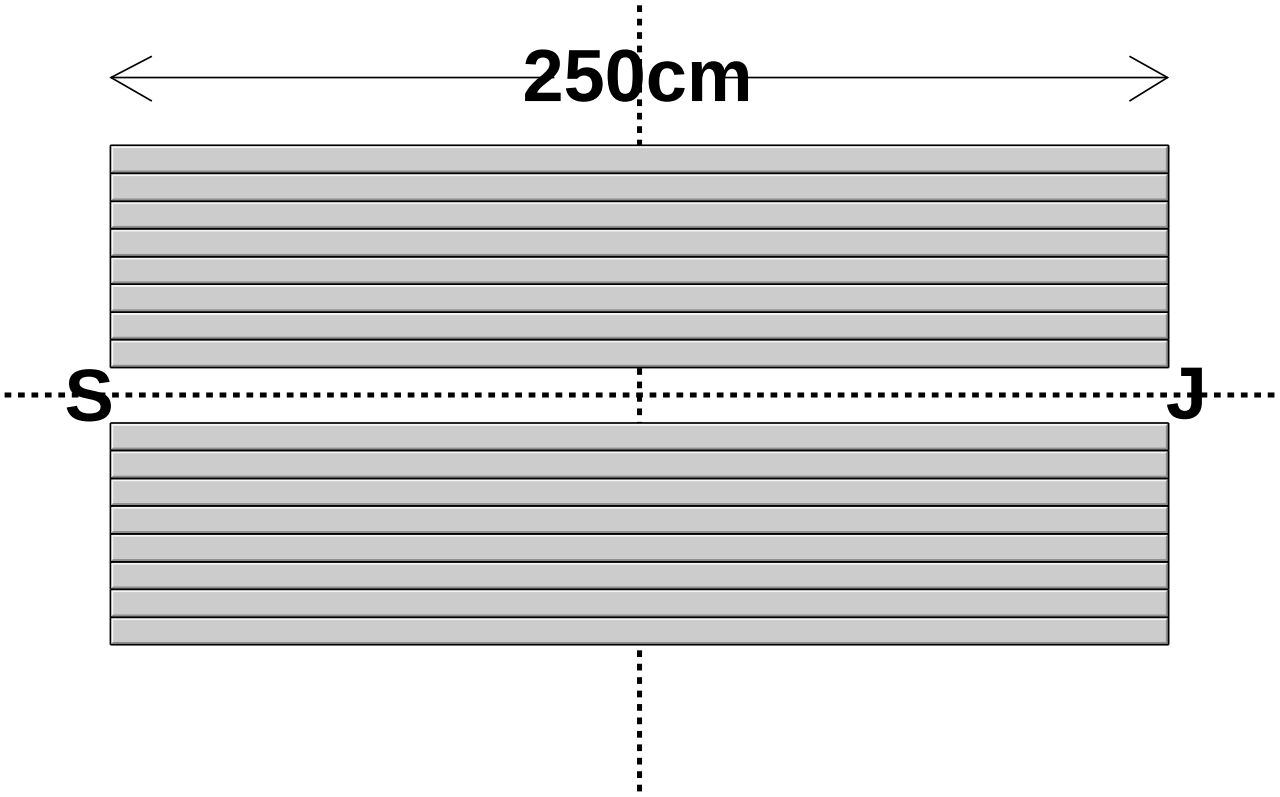

Figure 6: Scheme of the H3O hodoscope.

- Position: 20.97 m.
- One hodoscope with an upper and a lower part.
- only horizontal strips
- Double sided readout.
- Element size (width x depth x lenght): 70x9x2500 mm^3.
- Overlap: None
- Position and dimensions of hodoscopes strips in mm:

strip	low x	low y	len x	len y	comments
1	-1250	-630	2500	70	
2	-1250	-560	2500	70	
3	-1250	-490	2500	70	
4	-1250	-420	2500	70	
5	-1250	-350	2500	70	
6	-1250	-280	2500	70	
7	-1250	-210	2500	70	
8	-1250	-140	2500	70	
9	-1250	-70	0	70	these elements
10	-1250	-0	0	70	will be added in 2003
11	-1250	70	2500	70	
12	-1250	140	2500	70	
13	-1250	210	2500	70	
14	-1250	280	2500	70	
15	-1250	350	2500	70	
16	-1250	420	2500	70	
17	-1250	490	2500	70	
18	-1250	560	2500	70	

- Tubes: EMI.
- Reserved depth: ??? mm.
- Refurbished from old SMC hodoscope

3.5.2 H4

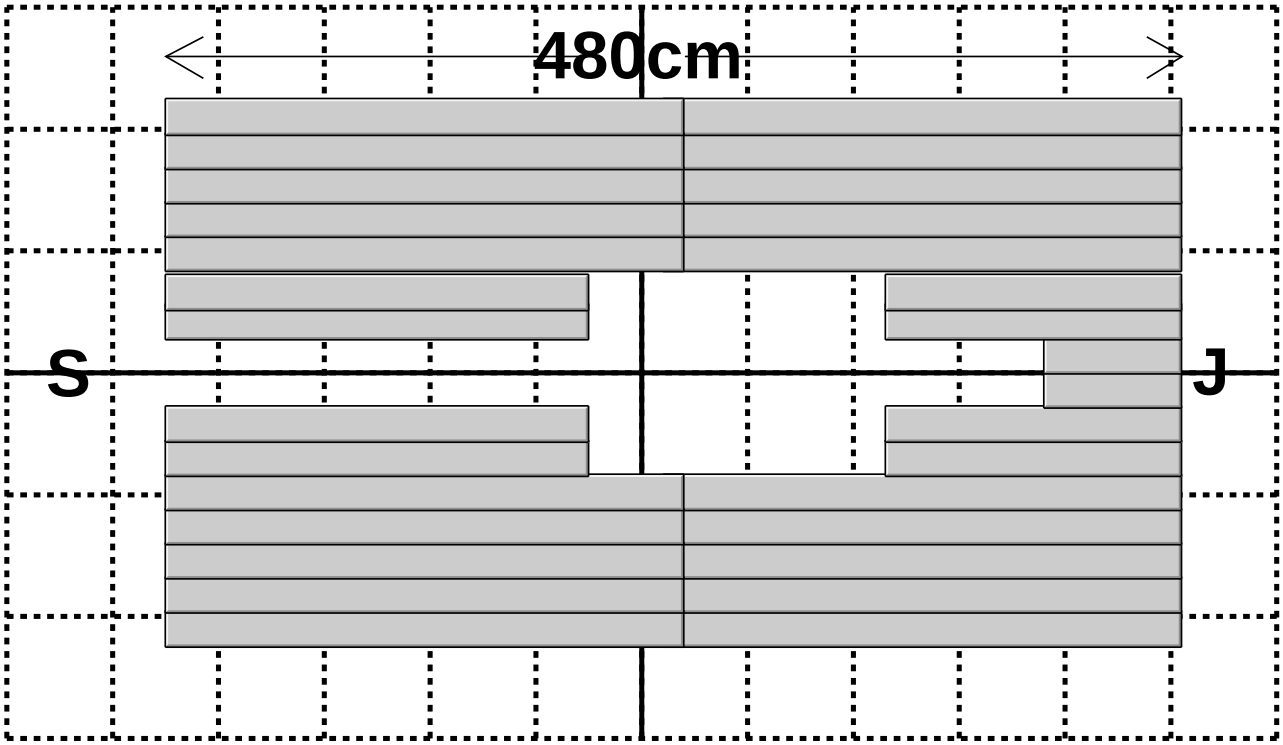

Figure 7: Scheme of the H4O hodoscope.

- Position: 40.05 m.
- Two hodoscope with an upper and a lower part, one for the jura side and one for the saleve side.

- Double sided readout.
- Element size (width x depth x lenght): 150x20xVariable mm^3.
- Overlap: 10 mm
- Position and dimensions of hodoscopes strips in mm:

strip	low x	low y	len x	len y	comments
H4 Jura					
1	100	-1125	2450	150	
2	100	-985	2450	150	
3	100	-845	2450	150	
4	100	-705	2450	150	
5	100	-565	2450	150	
6	1150	-425	1400	150	
7	1150	-285	1400	150	
8	1900	-145	650	150	
9	1900	-05	650	150	
10	1150	135	1400	150	
11	1150	255	1400	150	
12	100	415	2450	150	
13	100	555	2450	150	
14	100	695	2450	150	
15	100	835	2450	150	
16	100	975	2450	150	
H4 Salève					
1	-2250	-1125	2450	150	
2	-2250	-985	2450	150	
3	-2250	-845	2450	150	
4	-2250	-705	2450	150	
5	-2250	-565	2450	150	
6	-2250	-425	2000	150	
7	-2250	-285	2000	150	
8	-2250	-145	0	150	no elements foreseen
9	-2250	-05	0	150	no elements foreseen
10	-2250	135	2000	150	
11	-2250	255	2000	150	
12	-2250	415	2450	150	
13	-2250	555	2450	150	
14	-2250	695	2450	150	
15	-2250	835	2450	150	
16	-2250	975	2450	150	

- Tubes: XP2020 or EMI.
- Reserved depth: ??? mm.

4 Electronics

The electronics for the muon trigger has to cover different aspects: On one hand it has to provide triggers to the whole of the COMPASS experiment, on the other hand it has to assure the responses of the trigger detectors. The trigger generation requires the combination of position information, given by the strip number in the hodoscope, a scheme which is employed for both the quasireal and the DIS trigger. To get a clean trigger signal the time resolution in the coincidence matrices, which are employed to get a signal from the combination of hits in different hodoscope planes, have to be a good (xxxps).

Time resolution is of course not only an issue for the coincidence matrices, but also for the discriminators.[4] Since the ladder hodoscopes, the prime hodoscopes and especially the unprimed hodoscopes use rather long elements, we need to use double sided readout and mean timers in order to keep the absolute trigger timing in some bounds.

A survey of available discriminators lead us to modules produced by the IPN Orsay, which incorporate two constant fraction discriminators with about 125 ps time resolution and a mean timer with about 200 ps time resolution. These modules are described in section 4.3.1.

The coincidence matrices have to combine the signals of two sets of up to 32 signals into a trigger signal, with a coincidence overlap time of about 2 ns. Based on the experience with the coincidence matrices in the SMC experiment, which were built using standard ECL chips a new design was required. After a feasibility test we chose to make custom chips for the coincidence matrices, allowing for a simple design of the boards with only a few components. Also special chips as a means to control the timing on a nanosecond scale with sub-nanosecond resolution were implemented, so that we need to control the timing via cable lengths only down to a precision of 4 or 5 ns.

The digitization of the information of the trigger detectors is done via TDC's, pulse heights are irrelevant for the analysis of the trigger data, because they can't be used for particle identification and the timing is not correlated to the pulse height due to the use of constant fraction discriminators, as shown by test measurements. ADC's can be employed to monitor the pulse height spectra of programmed subsamples of the detector, thus allowing for continuous checks at reasonable cost.

The rest of this section gives a detailed discussion of the components and interplay of the components of the trigger electronics.

4.1 Signal Ways

The signals from the hodoscopes are run on fast (4ns/m) cables from the beam area to the trigger barrack. Figure 8 shows the location of the trigger hodoscopes, the hadron calorimeters (HCAL1 and HCAL2) and the barracks (HNB422 and HNB 429) which contain the trigger electronics.

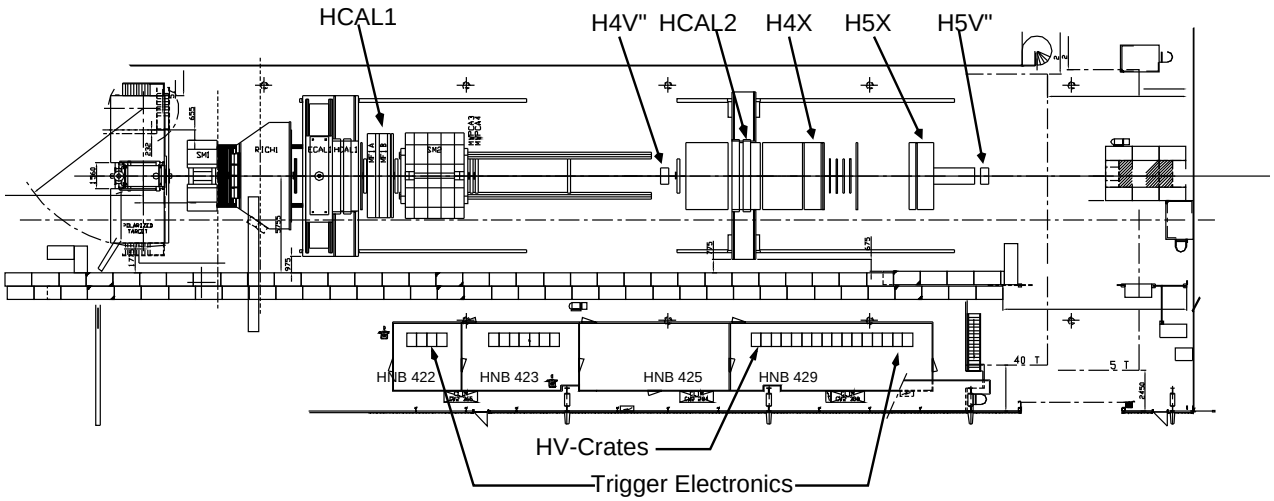

Figure 8: Geometrical layout of the Trigger hardware in the hall

The analog signals from the scintillation counters are (in the last racks in barrack HNB429) fed into the discriminator boards. From the discriminator boards the digital signals, which adhere to the LVDS standard [1],

[4] The Scintillators are covered in section **??**

are fed to TDC's, Scalers and to the coincidence matrices which combine the information from the H4 plane with that from the corresponding H5 plane. Figure 9 shows this scheme for one set of hodoscopes, while figure 10 shows the physical layout of the crates in their racks.

The larger hodoscopes H4VL, H4M, H5VL and H5M consist of scintillator bars which are read out on both sides, so there the relevant signals that are fed into the coincidence matrices and scalers are the outputs of mean timers, which are integrated into the discriminator boards, while the TDCs are still fed from the individual tube signals.

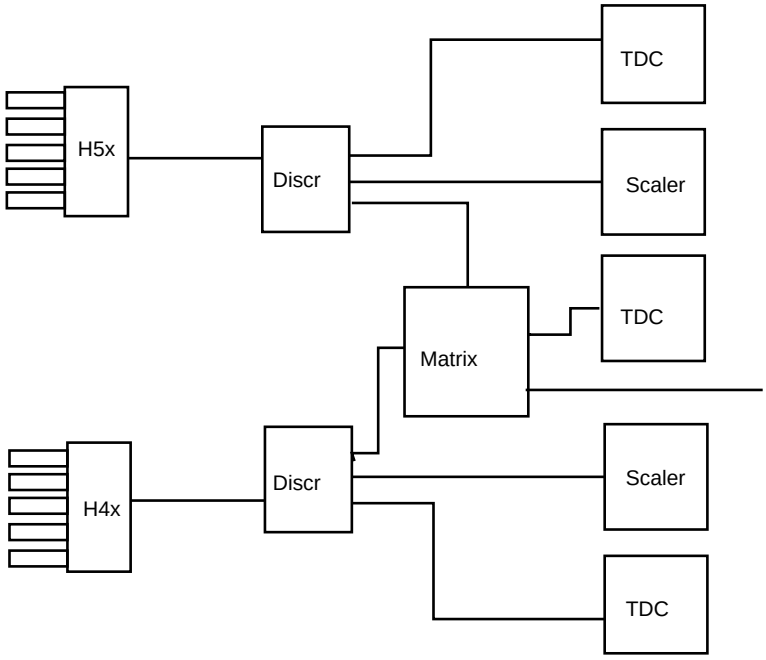

Figure 9: Trigger electronics overview

4.1.1 Signal standards

In the various parts of the electronic unfortunately a number of different signal standards have to be used. In this chapter a short list of all the standards used is given, together with basic descriptions of the signal parameters.

4.1.1.1 Analog signals The analog signals as they come out of the photomultiplier tube are single ended pulses, which are fed through 50Ω cables. The pulse heights will mostly vary between 50mV and some Volts, depending on the hit position in the counter, high voltage and some other parameters.

4.1.1.2 LVDS signals The standard digital pulses which are produced by the discriminator boards and the matrix boards and which are used by the TDCs are LVDS. LVDS [1] is an acronym for low voltage differential signaling, which shows the major features of the LVDS standard: It is a differential signal standard at low voltages, the high voltage ranging up to 1474 mV and the low voltage being at least 925 mV. The differential voltage lies between 250 and 400 mV, and the "offset" voltage is between 1125 an 1275 mV. The receivers must accept input voltages up to 2400 mV with a differential threshold of 100 mV. The logical one is defined by having the "+" line more positive than the "-" line.

A typical LVDS receiver has an input resistor of 100Ω. If the input of a LVDS receiver is not connected, shorted or in other ways improperly connected the output will go to a high level instead of uncontrolled behavior or oscillations as seen on some other logic families.

4.1.1.3 LVDS connectors On the cable plugs of the CERN catalog type 09.55.21.071.4 are used, this is the KEL type 8822E-068-171D and the Robinson Nugent type P50E-068S-TG.

$Id: rack-layout-hnb429.ips,v 1.3 2000/05/18 16:02:15 hannappe Exp $

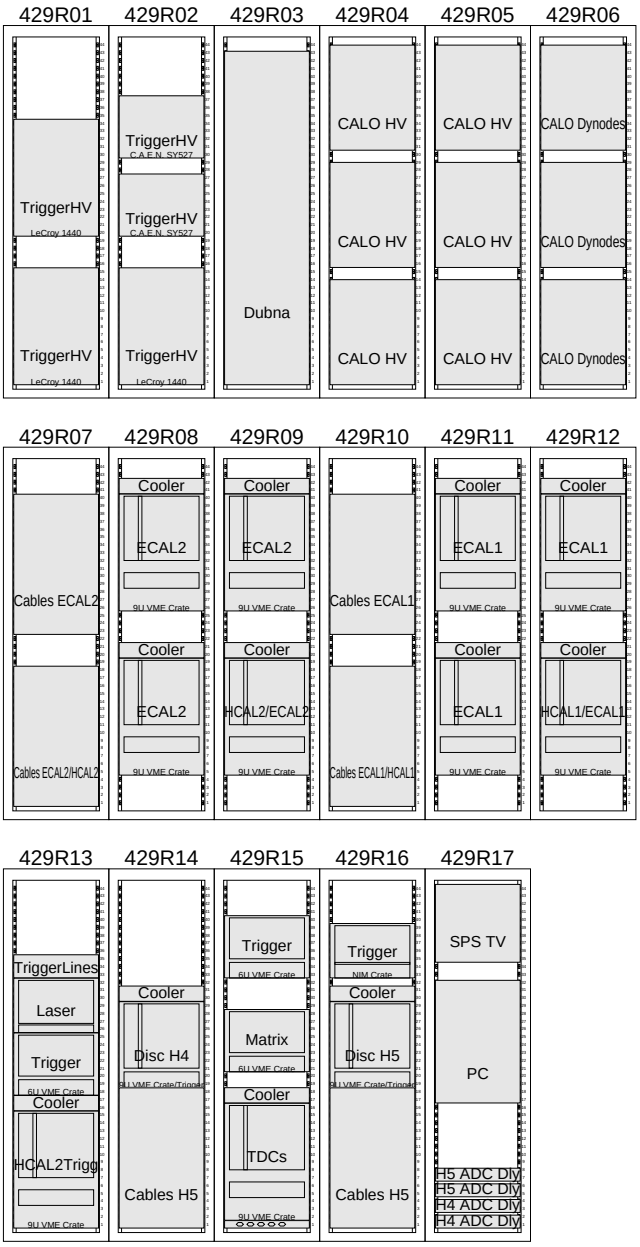

Figure 10: Rack layout in HNB 429

Signal	Polarity	Pin on Plug	Cable	Wire on Cable
1	+	A1	1	1
1	-	A2	1	2
2	+	B1	2	1
2	-	B2	2	2
3	+	A3	1	3
3	-	A4	1	4
4	+	B3	2	3
4	-	B4	2	4
		⋮		
31	+	A31	1	31
31	-	A32	1	32
32	+	B31	2	31
32	-	B32	2	32
–		A33	1	33
–		A34	1	34
–		B33	2	33
–		B34	2	34

Table 1: Assignment between channels, pins and wires for standard 68-pin lvds connections

On the boards we use the CERN type 09.55.21.368.0, which is KEL type 8831E-068-170LD, or Robinson Nugent type P50E-068P1-SR1-TG.

The cable that we use is standard 34-wire twisted pair flat cable, with 1.27 mm wire spacing. In the standard configuration two such cables attach to one plug, each cable then corresponds to one row of contacts on the plug. *Note that this assignment is not compatible with the plugs for high-density cables with 0.65 mm wire spacing, because the pairs of the twisted sections of the cable then do not match!*

This cabling scheme matches the LVDS to ECL converters built by the Freiburg group, as well as the TDC mezzanines for the catches. If the TDC mezzanines are used in high resolution mode, only every second pair of the twisted pair cables is used. This gives the opportunity to shield the active pairs by grounding the unused ones, thus lessening the effects of crosstalk on the cable.

The "+" line is the one connected to the first pin, called A1 in the notation used by the CERN catalog. So all the "+" lines are on odd numbered pins, the "-" lines on the even numbered ones. The odd numbered signals lie on the first cable, while the even numbered signals lie on the second cable. Table 1 shows this again, to make absolutely sure that there are no misunderstandings.

4.2 Readout

The readout of data of the trigger components is done via F1 TDCs [7], the TDC's sitting on Catch-boards [6]. In the first setup the TDCs will be used in the standard mode, which allows for 8 channels with 100 to 150 ps resolution per chip, giving a total of 128 channels per CATCH board. If necessary, the signals can be distributed in a way that allows to use the high resolution mode of the TDC's, with 50 to 75 ps, but only 64 channels per CATCH. Additionally the signals from the hodoscopes will go to scalers, which (probably) also will be implemented in the form of CATCH mezzanines. All this is shown for one set of hodoscopes in figure 9.

The scaler data will be useful both for normalizing and for quick monitoring of beam profiles and positions, giving also very quick response in case some channels start dying.

4.3 Discriminator Boards

In total (if all the hodoscopes are built) about 800 channels have to be fed into the discriminators, so a design was needed that allows for high density and computer controlled operation. In view of this, it was decided to use VMEBus modules with large form factor (9U × 400mm) for the discriminators, so that as many channels as possible could be housed within one crate and in the domain of one control CPU.

The discriminators used for the hodoscopes of the muon trigger are designed and built by the IPN Orsay, in the form of small daughter modules each carrying two constant fraction discriminator channels and (optionally)

one mean timer. These daughter boards are located on 9U-VME-Modules, which carry up to 32 daughter modules each, so that one VME-Card has 64 input channels, corresponding to 64 single-sided counters or 32 double-sided counters. The mother boards are designed in the Physikalisches Institut der Universität Bonn by A. Eyring for a first version, and by M. Henseler for the second version. The inputs are fed through the P3 connector, the outputs come to 6 connectors on the front panel.

An analog monitoring facility is provided, which brings a subset of the input signals on buffered analog outputs to further investigation. The analog monitor outputs will come to 8 lemo connectors on the front panel, and will be distributed in a way that allows for simultaneous watching of the two inputs of one Orsay module. This allows to have the signals of the longer counters with double sided readout simultaneously on ADC channels.

All discriminator channels can be individually inhibited and the thresholds are individually settable, with 256 steps between 0 and -2 V. There also exists a test pulsing facility, which allows to generate test pulses on the discriminator inputs, using the test inputs of the Orsay modules. Two lemo connectors on the front panel allow test pulses to be triggered externally. They are then distributed on the motherboard to the individual inputs, in a way that allows two different pulses to go to the two channels of one Orsay module.

4.3.1 The Orsay-Modules

The discriminator modules that are used for the trigger were developed by the IPN Orsay's electronics department[5]. Each module contains two constant fraction discriminators and an optional meantimer. The output signals are TTL for the meantimer and the individual CFDs, and an additional ECL output from the meantimer. The pin out is shown in figure 11.

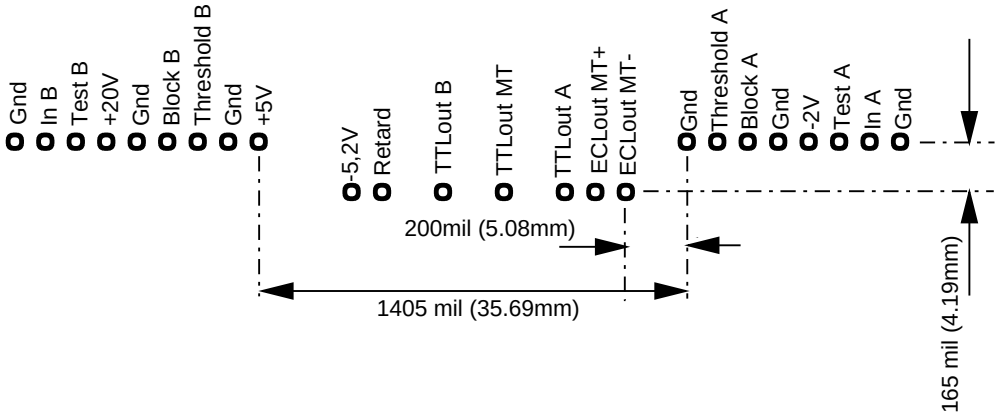

Figure 11: Pin out of the Orsay modules

Table 2 lists the pins of the modules, together with a short description of each pin.

4.3.2 VME-Interface

The VME interface of the discriminator boards consists mainly of a Xilinx chip with some SSI glue logic. The glue logic generates a chip select signal if the board is addressed in it's assigned address range in the short IO space of the VME bus. A special design is employed to allow loading the Xilinx configuration over the VMEBus. This is done by having a simple VME interface done with standard TTL/CMOS chips, which consists mainly of two equality comparators, that detect accesses to the address range assigned to the board. While the FPGA is not loaded writes to the base address load one byte of the configuration data into the FPGA in the so called slave peripheral mode as soon as the FPGA is ready it takes over the responses to the VME accesses and maps its internal registers to the VMEBus. This kind of VME interface in various implementations is used on all the VME boards, the three versions of the discriminator board as well as on the matrix boards.

[5] http://ipninfo.in2p3.fr/ipn/technique/sep-en.html

Pin-Name	Description
Gnd	
In B	Signal input for the B discriminator
Test B	Test input for the B discriminator, Test pulse has to be simply an ECL pulse, negative phase, the leading edge being active, it results in a pseudo physical pulse current-injected at the CFD input and about 800mV amplitude.
+20 V	Voltage to supply the ramp generator of the meantimer stage, may be varied a bit to adjust the meantimer range, but should not be too far from the 20V value to keep the precision.
Gnd	
Block B	Inhibit for the B discriminator, 0V=Inhibit, 5V=Enable
Thres. B	Threshold for the B discriminator, between 0 and -2 V
Gnd	
+5 V	Positive supply Voltage, 125mA
-5.2 V	Negative supply Voltage, 250ma
Retard	Threshold for the mean timer stage, between +0.55V and +3V. Sets also the delay of the mean time stage.
TTLout B	Output of the B discriminator, TTL levels
TTLout MT	Output of the mean timer, TTL levels
TTLout A	Output of the A discriminator, TTL levels
ECLout MT+	Output of the mean timer, ECL normal level
ECLout MT-	Output of the mean timer, ECL inverse level
Gnd	
Thresh. A	Threshold for the A discriminator, between 0 and -2 V
Block A	Inhibit for the A discriminator, 0V=Inhibit, 5V=Enable
Gnd	
-2 V	ECL auxiliary Voltage, 100mA
Test A	Test input for the A discriminator
In A	Signal input for the A discriminator
Gnd	

Table 2: Pin description of the Orsay modules

If a VME sysreset is issued over the bus the Xilinx will be re-initialized and a new download of the FPGA data becomes necessary. The download of the FPGA data is done by a VME cpu in the crate, or alternatively by any kind of VME master.

4.3.3 Prototype version

A prototype of the discriminator board has been built, which uses the 6U-VME-Form factor and houses up to 8 daughter boards.

The VME interface of the prototype board is built with the Xilinx XC3000 FPGA [5].

4.3.4 Semi-final Version

The final version of the discriminator board became available mid may 2000. Its inputs go via the P3 connector, which is a CD128M abcd VG-Connector. This is matched with a RD128 abcd connector on a small transition module. Table 3 shows the pin assignment for the P3 connector. In this table the Channel refers to the channel number on the output connector, the TBnum is the number of the input line in the schematics of the board and on the transition modules.

Pin	Row	Channel	a/b	TB num	Pin	Row	Channel	a/b	TB num
32	d	1	a	1	32	a	1	b	2
31	d	2	a	3	31	a	2	b	4
		⋮					⋮		
2	d	31	a	61	2	a	31	b	62
1	d	32	a	63	1	a	32	b	64

The Rows b and c of the connector carry the ground returns for the input signals (in fact they are connected to the ground plane).

Table 3: Discriminator board input pin assignment

The modules also allow to monitor the analog signals of the inputs by routing a switchable subset of them to monitor outputs. This is done by buffering the signals with MAX4223 amplifiers that have switchable outputs. Groups of eight amlifiers go to the same output line, so that one of eight signals can be monitored at a time. Table 4 shows the assignment of the monitor line a0 to b3 to the input signals.

Channel	a/b	TBnum	Monitor	Channel	a/b	TBnum	Monitor
1	a	1	a0	17	a	33	a1
1	b	2	b0	17	b	34	b1
2	a	3	a0	18	a	35	a1
2	b	4	b0			⋮	
		⋮		24	b	48	b1
8	b	16	b0	25	a	49	a2
9	a	17	a3	26	b	50	b2
9	b	18	b3	27	a	51	a2
10	a	19	a3			⋮	
		⋮		31	b	62	b2
16	a	31	a3	32	a	63	a2
16	b	32	b3	32	b	64	b2

Table 4: Correspondence of monitor outputs and input signals

It is possible to change this assignment, but only at the expense of quite a lot of work on the discriminator boards, because a change there would require to create a new cabeling of the analog output lines by hand.

Due to problems during the production and some less than optimal points in the layout of these boards they were redesigned, and by summer 2001 a new final version became available.

4.3.5 Final Version

The new "final version" of the discriminator boards is a layout with 12 layers, 4 of them being power planes and 8 signal layers. The board stack-up is described in table 5. This board stack-up allows to run the LVDS

18μm	Cu	component side
66μm	Prepreg	
66μm	Prepreg	
35μm	Cu	power plane 1
200μm	FR4	
35μm	Cu	signal layer 3
115μm	Prepreg	
115μm	Prepreg	
35μm	Cu	signal layer 4
200μm	FR4	
35μm	Cu	power plane 2
66μm	Prepreg	
66μm	Prepreg	
35μm	Cu	signal layer 5
360μm	FR4	
35μm	Cu	signal layer 6
66μm	Prepreg	
66μm	Prepreg	
35μm	Cu	power plane 3
200μm	FR4	
35μm	Cu	signal layer 7
115μm	Prepreg	
115μm	Prepreg	
35μm	Cu	signal layer 8
200μm	FR4	
35μm	Cu	power plane 4
66μm	Prepreg	
66μm	Prepreg	
18μm	Cu	solder side

Table 5: Discriminator board stack-up

output lines to be done in broadside coupled layout, i.e. the two traces for one differential pair run on two adjacent layers with identical layout. The trace widths and dielectric thickness have been adjusted to achieve a differential impedance of 100Ω and an single-ended (trace to ground) impedance of 50Ω. Measurements with an oscilloscope used as a time domain reflectometer have shown that this goal was achieved. The thick dielectric layers required an overall thickness of the board of 2.5mm, which in turn made milling of the upper and lower borders of the boards to the more conventional thickness of 1.6mm necessary to keep the ability to put the boards into the rails of ordinary crates.

The thresholds of the discriminator modules are set by MAX510 quad DACs, which are serially controlled and offer 8 bits resolution. In connection with the threshold range from 0 to -2 Volts this results in 7.8mV threshold resolution. All sixteen chips on a board form a single serial chain, and the reference voltages for the DACs are taken directly from the -2V plane.

The meantimer thresholds are controlled by MAX5250 quad DACs, also forming a serial chain and offering 10 bits of resolution, with a maximum meantimer threshold of 3.3 Volts this gives a 3.2mV resolution. The reference voltages are taken from a precision 3.3V shunt regulator (Zetex zrc330) for each DAC individually.

The enable inputs of the 64 discriminator channels are wired to the parallel output of a shift register consisting of 8 74HC595, in like manner the enable inputs of the buffer amplifiers for the analog monitoring are fed by a shift register made from 8 74HC595. A second set of the shift register control signals (Shift Clock, Shift Data and Load Data) is available for both shift registers on a 12-pin connector, so that a front panel with LEDs showing the disabled channels and the currently active monitor channels can be connected.

The analog input signals arrive at the P3 connector or at the P2 and the P3 connector, and run via thin

boundary␣sc
JTAG

coaxial cables (cable TYPE C-50-1-2, CERN SCEM 04.61.11.110.6) from a patch field immediately adjacent to the backplane connectors to the input sections of the discriminator modules. All the cables are kept at the same length so that the timing for all channels is equal. The use of coaxial cables for the analog input lines offers over the more easily manufactured PCB tracks the advantage of less crosstalk and also the possibility to choose the input pin assignment at assembly time rather than at design time. This flexibility on the input pin assignment allows the board to be used both with one 128-Pin P3 transition module for 64 channels as used by the trigger group as well as with two 64-Pin P2/P3 transition modules as used for the calorimetry ADCs.

The analog monitor outputs are also connected via coaxial cable rather than PCB traces, also allowing for flexibility in the grouping of the multiplexed channels.

Table :discrv2-channels shows the default connections chosen for the discriminator boards with all intermediate namings used.

on cables	on transition module	on P3 conn.	on orsay module	output
1	in 64	a 31	A 0	O1,1
2	in 62	a 30	A 1	O1,2
		⋮		
31	in 4	a 1	A 30	O1,32
32	in 2	a 0	A 31	O1,32
33	in 63	d 31	B 0	O6,1
34	in 61	d 30	B 1	O6,2
		⋮		
63	in 3	d 1	B 30	O6,31
64	in 1	d 0	B 31	O6,32

Table 6: Channel assignment of the version 2 discriminator boards

4.4 Coincidence Matrices

The coincidence matrices are built in the form of classical 6U VME modules, one module providing a 32 by 32 coincidence matrix with adjustable timing for each input channel and each output channel. The input signals are brought into the boards via the connectors discussed in section 4.1.1.3, go via differential lines to lvds to ttl converters. Once in ttl level the signals are fed through the custom delay chips, which allow to adjust the delay of the signals with 8 ns range and 250 ps resolution. The delay chips are also used for pulse shaping, so that the width of the coincidence window can be set here. Then the shaped and timed signals go to the matrix chip, where the coincidences between the rows and columns are made. On the output of the matrix we have 32 signals, one for the or of each row, that are again fed through a delay chip to get shaped signals of well defined length, and then via ttl to lvds converters again to the output connector. The matrix chip produces also an overall "or" signal, which is the or of all the 32 row outputs, which goes to an extra output.

4.5 Custom chips

The custom chips for the matrix boards were developed by M. Henseler in the Physikalisches Institut der Universität Bonn. They are implemented in the 0.8μm CMOS process by AMS[6] [4].

Some features are common to both the matrix and the delay chip, such as the boundary scan.

4.5.1 Boundary scan

For testing purposes both kinds of custom chips are equipped with a boundary scan facility, inspired by the JTAG standard. It has the same kind of boundary scan cells as a JTAG device, shown in figure 12, but for simplicity the state machine was left out and the necessary control pins are directly available.

The operation of the boundary scan feature is governed by the pins called BSena, BSshift, BSclk, BSupd, BSsi and BSso. All the scan cells build a long shift register, the `SerIn` line of each scan cell is connected to the preceeding ones `SerOut` line, while the first SerIn connects to the BSsi pin of the chip and the last SerOut is connected to BSso. To shift data through this shift register the BSshift pin, which is connected (via a buffer)

[6] http://www.imec.be:8000/europractice/on-line-docs/prototyping/ti/ti_cye.html

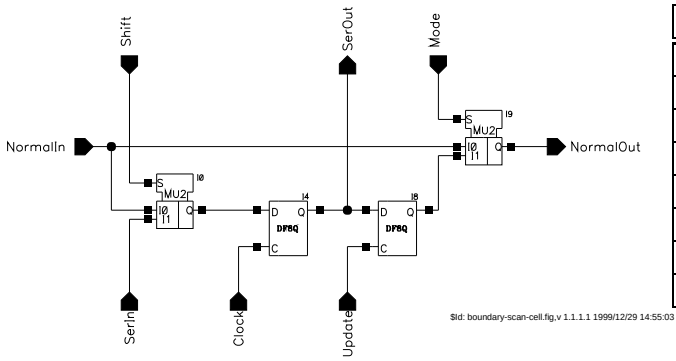

Scan cell line	External Pin
SerIn	BSsi
SerOut	BSso
Shift	BSshift
Clock	BSclk
Update	BSupd
Mode	BSena
NormalIn	Inpin/ChipOut
NormalOut	ChipIn/Outpin

Figure 12: Schematics of a boundary scan cell

to all the Shift lines of the individual boundary scan cells, must be pulled high, and the BSclock, connected to all the Clock lines of the cells, must be pulsed once.

If the Boundary scan cell sits on an input to the chip, the status of the input line can be sampled at any time by providing a clock to the BSclock pin, if BSshift is inactive (low). At the same time the status of the output lines of the chip is also sampled in the cells connected to the outputs.

The BSena pin, which is connected to the Mode lines of the scan cells, is used to switch the device from normal mode (BSena low) to boundary scan mode (BSena high). In the boundary scan mode the chip's input lines are decoupled from the input pads. They now get their values from the second flip-flop of the boundary scan cells. Also the output pads of the chip are decoupled from the output lines, but get their value from the last flip-flop. This last flip flop is loaded from the shift register by a clock pulse on the BSupd pin, which is connected to the `Update` lines of all the cells.

Thus the inputs to the chip and the outputs from the chip may be sampled at any time without intrusion to the chips operations. Providing simulated input signals and driving the outputs of the chip via boundary scan is of course limited to extra test sessions.

In the following schematics the symbol for the boundary scan cells is called `IB55BScan`. Detailed lists of the boundary scan pins are included in the chapters describing the individual chips.

4.5.2 Matrix-Chips

The Matrix chip comes in a 120 pin PGA socket, figure 13 shows the pin-out, while table 7 lists the order of the boundary scan cells.

The matrix chip, as can be seen in figure **??**, consists of several blocks, which are the matrix proper, two coincidence logic blocks for the inputs, and the periphery logic.

The matrix proper is built from 32 matrix lines, shown in figure 14, each of which contains the coincidences between one row and each of the 32 columns.

The 32 outputs of the 32 matrix lines are fed directly to the output boundary scan cells Out0 to Out31, and are also or'ed together and go to OutAll.

The coincidence logic blocks for the inputs, shown in figure 15, can be used for overlapping counters, to increase the spatial resolution. This logic blocks can be switched separately for rows and columns, if the respective input (RowMode oder ColMode) is high, the overlap logic is enabled, if low, it is bypassed and the matrix behaves in it's simple mode.

Each one of the 1024 coincidences of the matrix is made according to the schematic shown in figure 16. A 3-input "and" makes the coincidence between the pulse from the row and column and a level from a shift registers flip-flop.

The shift register flip flops are a special space-saving design, shown in figure 17. They must be clocked with a two phase clock, `Clkq` and `Clkd`, where `Clkd` must precede `Clkq` by some nanoseconds, and stay on also some nanoseconds longer. Experience shows that the matrix chips hold the pattern written into the flip-flops for at least half a minute even without power supply.

The input of the shift register is wired to the pin `DSin` or `SI` (44, N6), the output of the shift register is wired to the pin `DSout` or `SO` (43, M6)[7].

[7]Unfortunately in different schematics different names were used for the same pin, so both are given here

1	Col02	19	Row16	37	ColMode	55	Out12	73	Out30	91	Col15
2	Col01	20	Row15	38	DSout	56	Out13	74	Out31	92	Col14
3	Col00	21	Row14	39	DSin	57	Out14	75	Col31	93	Col13
4	Row31	22	Row13	40	Clkd	58	Out15	76	Col30	94	Col12
5	Row30	23	Row12	41	Clkq	59	Out16	77	Col29	95	Col11
6	Row29	24	Row11	42	OutAll	60	Out17	78	Col28	96	Col10
7	Row28	25	Row10	43	Out00	61	Out18	79	Col27	97	Col09
8	Row27	26	Row09	44	Out01	62	Out19	80	Col26	98	Col08
9	Row26	27	Row08	45	Out02	63	Out20	81	Col25	99	Col07
10	Row25	28	Row07	46	Out03	64	Out21	82	Col24	100	Col06
11	Row24	29	Row06	47	Out04	65	Out22	83	Col23	101	Col05
12	Row23	30	Row05	48	Out05	66	Out23	84	Col22	102	Col04
13	Row22	31	Row04	49	Out06	67	Out24	85	Col21	103	Col03
14	Row21	32	Row03	50	Out07	68	Out25	86	Col20		
15	Row20	33	Row02	51	Out08	69	Out26	87	Col19		
16	Row19	34	Row01	52	Out09	70	Out27	88	Col18		
17	Row18	35	Row00	53	Out10	71	Out28	89	Col17		
18	Row17	36	RowMode	54	Out11	72	Out29	90	Col16		

Table 7: List of the Boundary Scan cells of the Matrix chips

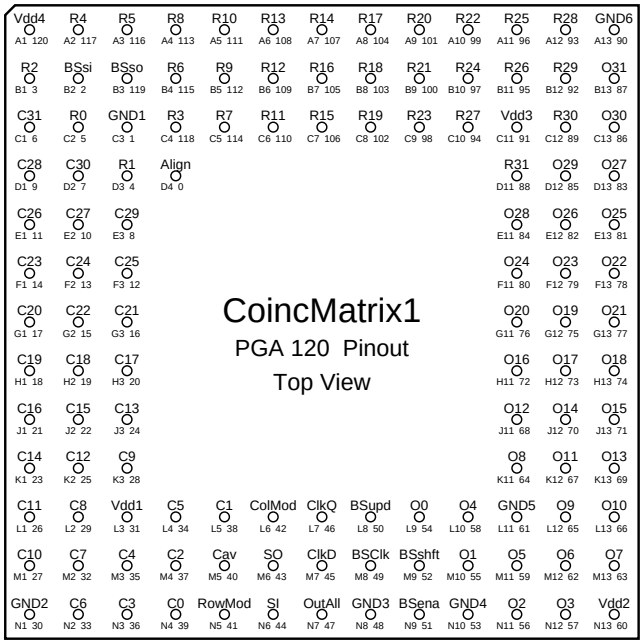

Figure 13: Matrix-Chip pin-out

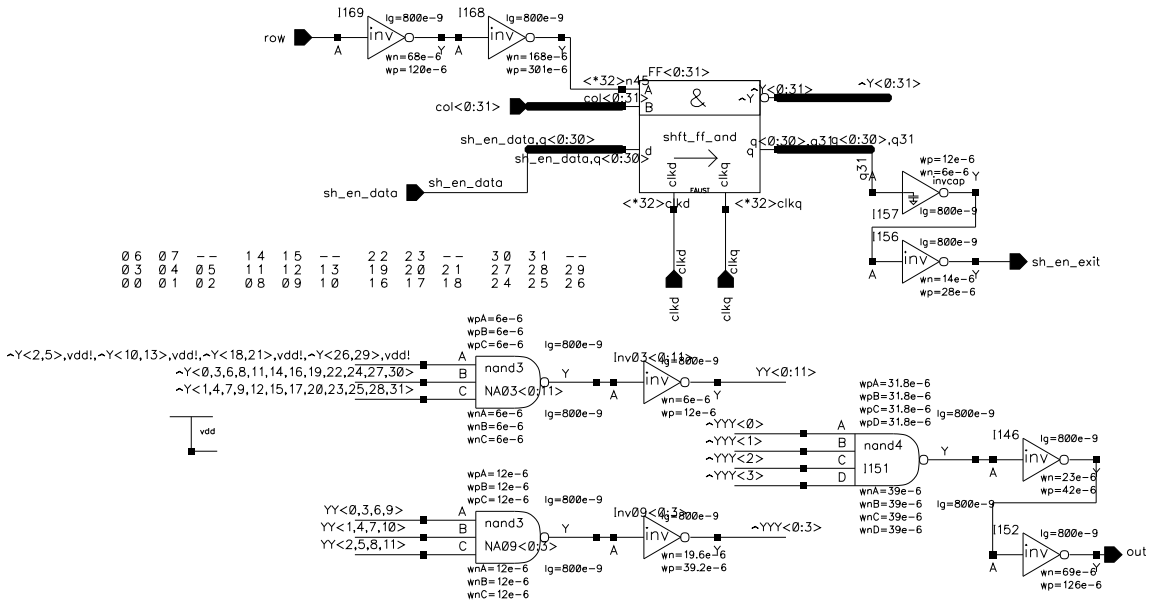

Figure 14: Matrix-Chip line

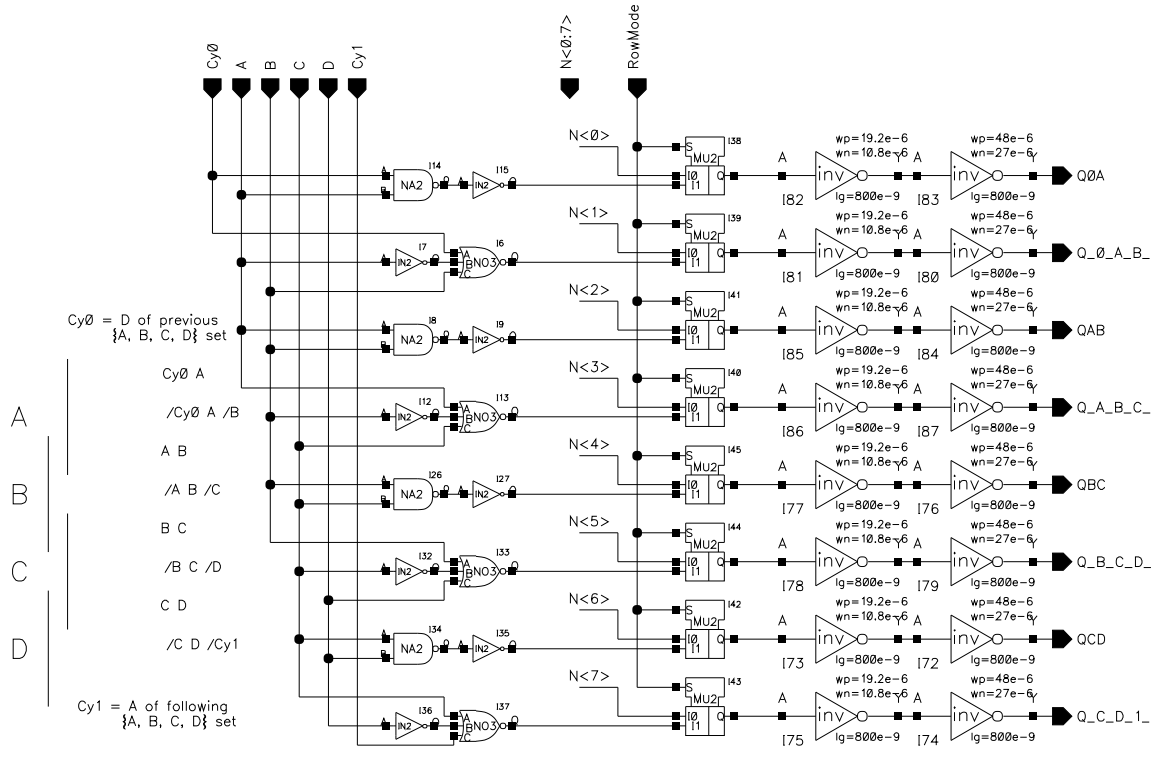

Figure 15: Matrix-Chip overlap logic

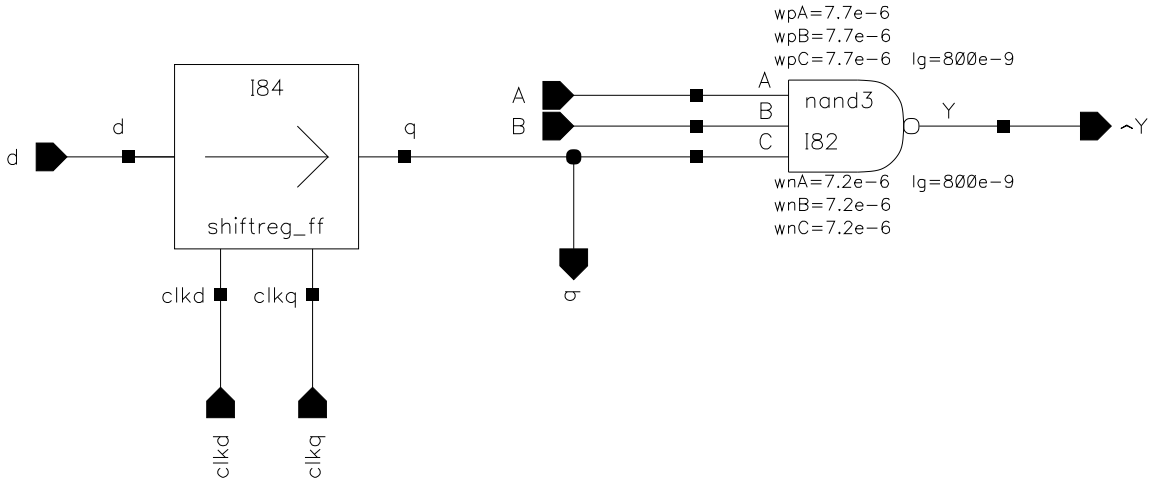

Figure 16: Matrix-Chip single coincidence

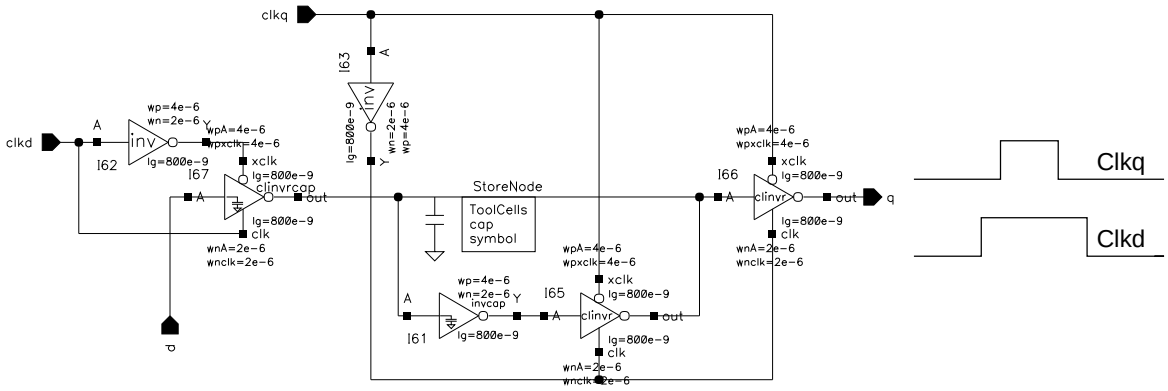

Figure 17: Coincidence matrix configuration flip-flop

4.5.3 Delay-Chips

The delay chip comes in a 68 pin PLCC or JCLCC package, figure 18 shows the pin-out, while table 8 lists the order of the boundary scan cells.

1	In15	9	In07	17	Dclk	25	Out02	33	Out10
2	In14	10	In6	18	PassData	26	Out03	34	Out11
3	In13	11	In05	19	MonoMode	27	Out04	35	Out12
4	In12	12	In04	20	MonoDly	28	Out05	36	Out13
5	In11	13	In03	21	DataExit	29	Out06	37	Out14
6	In10	14	In02	22	DelayData	30	Out07	38	Out15
7	In09	15	In01	23	Out00	31	Out08		
8	In08	16	In00	24	Out01	32	Out09		

Table 8: List of the Boundary Scan cells of the delay chips

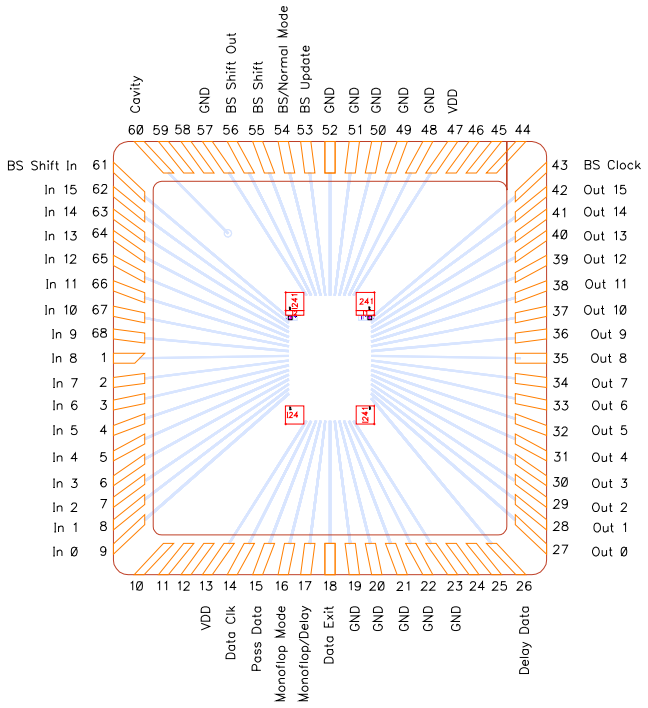

Figure 18: Delay-Chip pin-out and bonding

The delay chip, as can be seen in figure 19, consists of a sixteen-fold delay unit and the periphery logic.

Each of the sixteen delay channels consists of a number of configurable sub cells, shown in figure 20. The output of the delay channel comes from a multiplexer that selects if the channels does pulse forming or not. If no pulse forming is selected via the `Mono_Delay` line, the output pulse is the same as the input pulse, only delayed. If pulse forming is selected, the output pulse is the output of an R/S latch, which is set by the undelayed input pulse and reset by the delayed input pulse, so that the duration of the output pulse is (roughly) the delay set in the second 8 nanosecond delay stage of the channel. This configuration using the R/S latch ensures that the output pulse length is independent of the input pulse length, as pulses can both be stretched and shortened by this design. To eliminate the possibility of hangs that may be caused by a very short input pulse which only sets the latch but fails to reset it (after all it must travel for resetting through the delay chain) the inverter in front of the delay chain has different gate sizes from the other inverters to make it more sensitive to short pulses and thus always guarantee resets.

The first 8 nanosecond delay stage of a delay channel can be switched with the `Mono_Mode` line into two different functions. One, with `Mono_Mode` high, uses the first delay stage to delay the pulse and the second one for pulse forming, the other, with `Mono_Mode` low, uses both delay stages for the pulse forming.

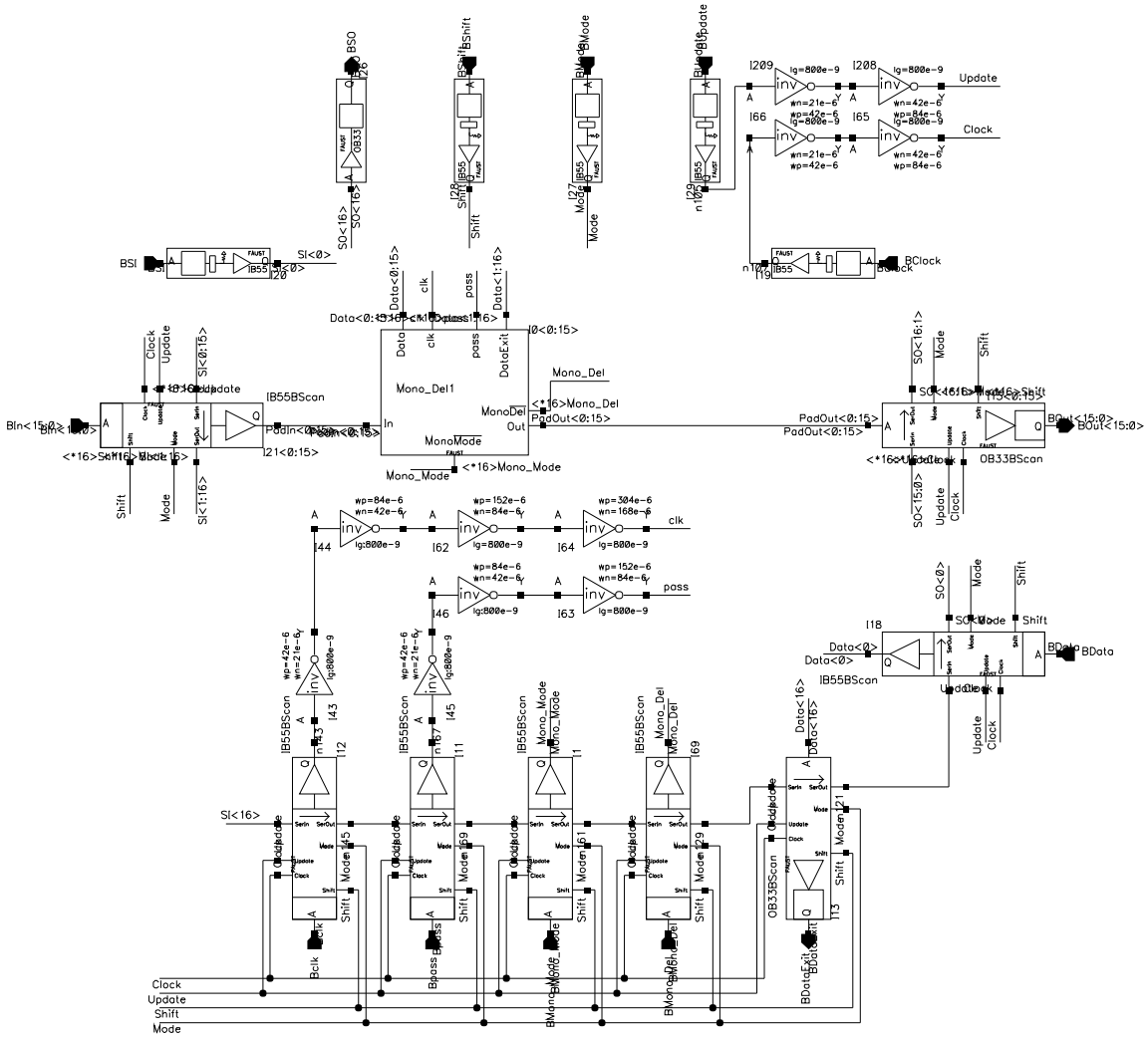

Figure 19: Delay-Chip schematic

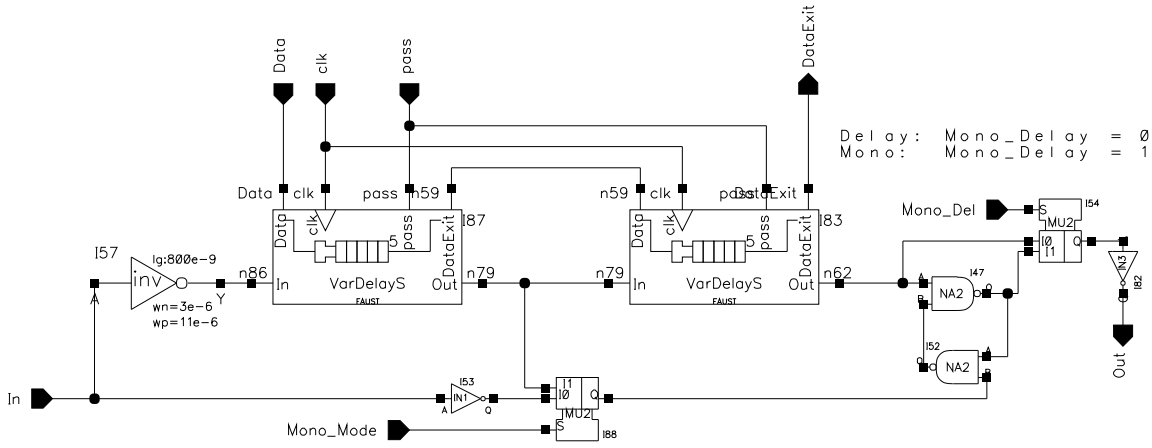

Figure 20: Delay-Chip, one channel

Table 9 shows the possible operation modes of the delay chip. The `Mono_Mode` and the `Mono_Del` operate on one complete chip, so that all 16 channels are always in the same operation mode.

`Mono_Mode`	`Mono_Del`	Delay Range	Pulse length range
X	L	16ns	follows input
L	H	fixed	16ns
H	H	8ns	8 ns

Table 9: Configurations of the delay chip

The single 8 nanosecond delay stages work as shown on figure 21. Five chains of inverters, with 2, 4, 8, 16 and 32 inverters each can be selected by the use of five multiplexers, so that the overall delay can be set to that of any even number of inverters from none to sixty-two. The resolution of this delays is thus given by the delay of two inverters, and is 250ps per step, amounting to 8ns for the full chain.

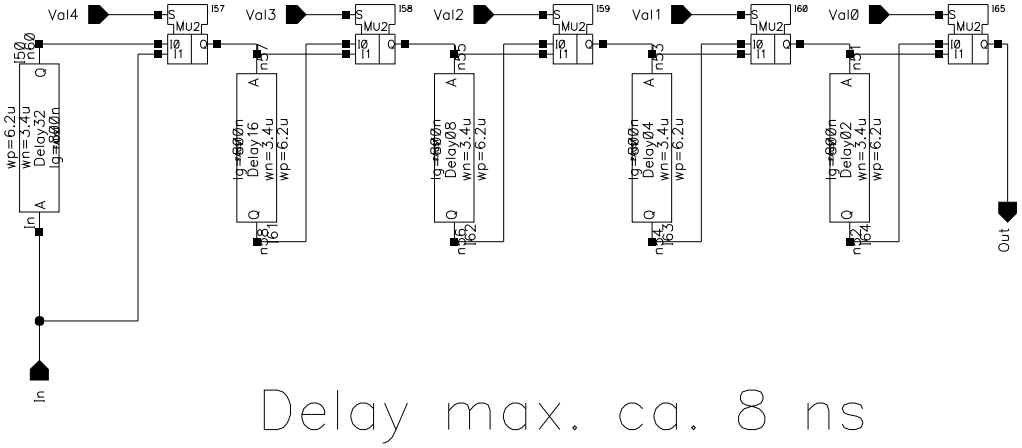

Figure 21: Delay-Chip delay only

The configuration flip-flops of the delay chip shown in figure 22 are far more comfortable than the of the matrix chip, since space was no so scarce here. The shift register that is formed from all the configuration bits ($16 \times 2 \times 5$ bits) is shifted with the one-phase clock `shift`, wired to the pin `Data_Clk` (14). The configuration data which really drive the multiplexers are stored in another set of flip-flops, which can be loaded from the shift-register with a clock signal on the `pass` line, wired to the pin `Pass_Data` (15).

The input of the shift register is wired to the pin `Delay_Data` (26), and the output of the shift register goes to the pin `Data_Exit` (18).

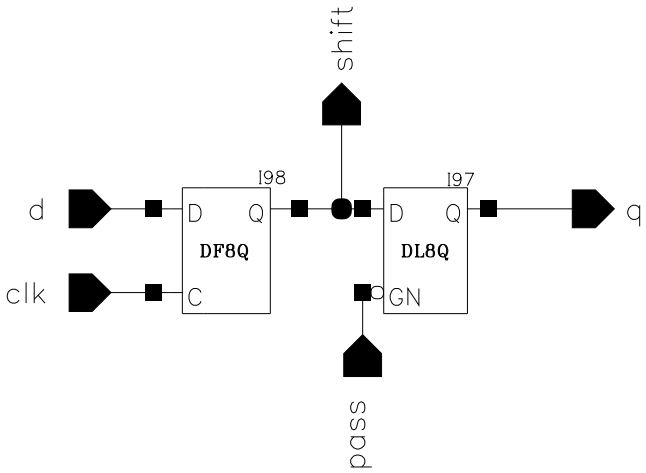

Figure 22: delay chip configuration flip-flop

4.6 Grounding

This section essentially describes the grounding, or rather the ground paths of the muon trigger equipment, as it is known today (that is the dawning of the new millennium, i.e December 2000).

The trigger logic sits like a spider with it's body in the barrack HNB429 and it's legs spread out from the very end of the experiment (H5VI) to the beam line (A veto counter in the vicinity of the last quadrupules).

Figure 23 shows an overview of the trigger grounding scheme.

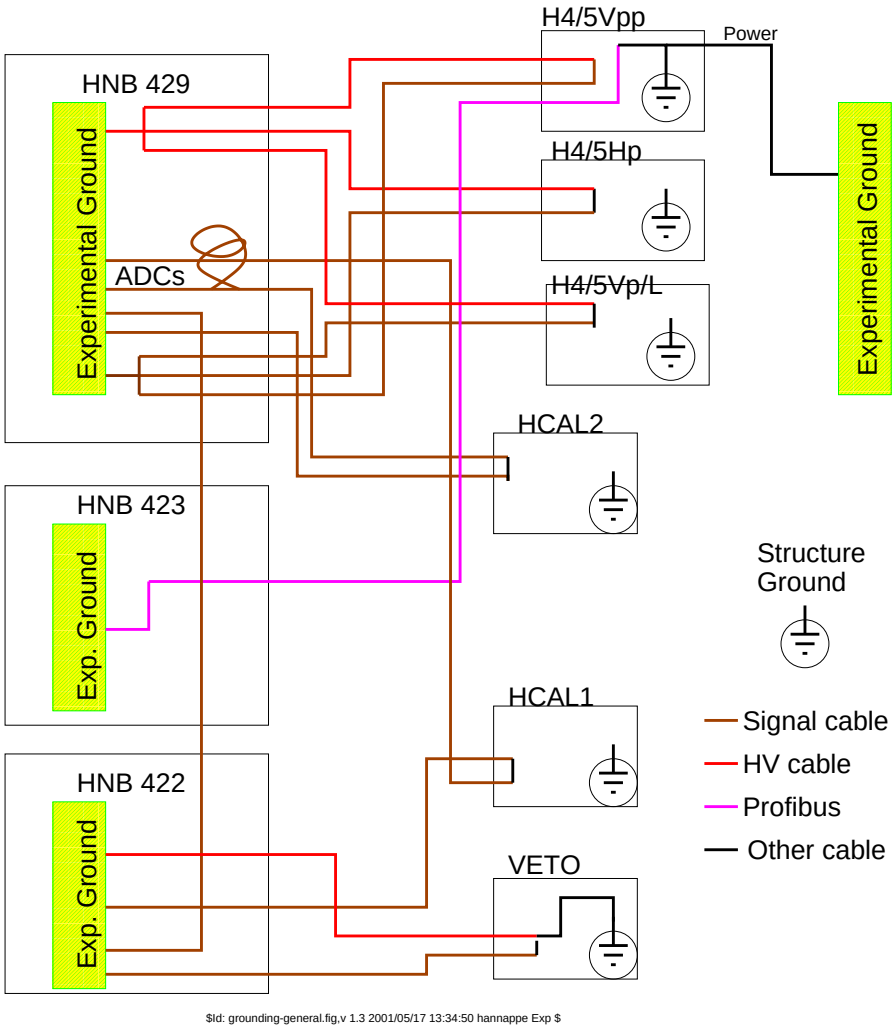

Figure 23: general grounding of the trigger

4.6.1 H4VI, H4HM, H5VI and H5HM

The tubes used for the small size scintillators, Phillips XP2900 and Hamamatsu R7400, are housed in aluminum tubes which have no connection to the high voltage or signal grounds. Therefore the hodoscopes H4VI, H4HM, H5VI and H5HM have the following grounding scheme:

- The HV crates sit in 429R01 and 429R02 and are there (of course) connected to the experimental ground. The HV lines then go to the hodoscopes, where the plugs at the end are screwed to a aluminum plate which is connected to the structural ground. No rule without exception: The hodoscopes H4HM and H5HM have no such aluminum plate at present, i.e. there there is no connection between signal ground and structural ground at the hodoscope.

- From the HV plugs on the aluminum plate at the hodoscope frame short cables go into the tube housings, where they are soldered to the PM bases.

- The signal cables start as short thin cables at the PM bases, again with no connection to the housing, and go to connectors at the beginning of long thick signal cables, which will carry the signals into the barrack.
- The long thick signal cables have at their beginning at the hodoscopes no connection to the structural ground, but end on connector plates in the barracks where they are then connected to ground. This ground connection is done in 429R14 and 429R16.
- The frames of H4VI and are motorised, and thus a ground connection from their structural ground to the experimental ground exists, via the power line from the outlet on the shield wall beside HCAL2 to the electronics for the motorisation. Also a connection via the shield of the Profibus cable that provides a control connection to the motor electronics exists between the DCS PC in HNB423. *This is also true for the other Profibus field couplers!*

4.6.2 Ladder and vertical prime hodoscopes

The vertical prime hodoscopes H4VM and H5VM use tubes different from those used in the hodoscopes described in 4.6.1, with the important difference in terms of grounding is the connection between signal/HV ground and PM housing. Therefore these hodoscopes have an additional connection to the structural ground at their PM housings, while the routing of the cables is the same as for the other hodoscopes, especially H4HM and H5HM, which hang at roughly the same positions.

4.6.3 Hadron calorimeter trigger

The calorimeter trigger electronics has several stages, the first one consists of summing boxes which are located on the downstream side of the calorimeters. From the boxes shielded twisted-pair cables run to the second stage, which sums up the signals of the boxes. The signal ground of the boxes is connected to the shield of the cables that go to the next summing stage in the barracks.

These second-stage cards are housed in 422R01 for HCAL1 and in 429R17 for HCAL2.

4.6.4 Veto counters

The veto counters that were used in 2000 had a connection between structural ground and signal/HV ground on the PM base housing. They were supplied with HV from a crate in 422R03, the signals were discriminated in 422R04 and sent from there to 429R15.

5 Hodoscope Hardware

5.1 Test of the scintillators for the prime system

For the choice of the scintillator material for the prime system a series of tests was done with the 855 MeV electron beam of the Mainzer Microtron MAMI. The purpose of these tests was to the determine the time resolution and the light attenuation length for different scintillator materials. The tests were done in June, October and December 1999.

5.1.1 Experimental setup

The setup scetched in fig.24 consisted out of a scintillator cross to trigger on an incoming electron and the scintillator under test was mounted on a moveable table.

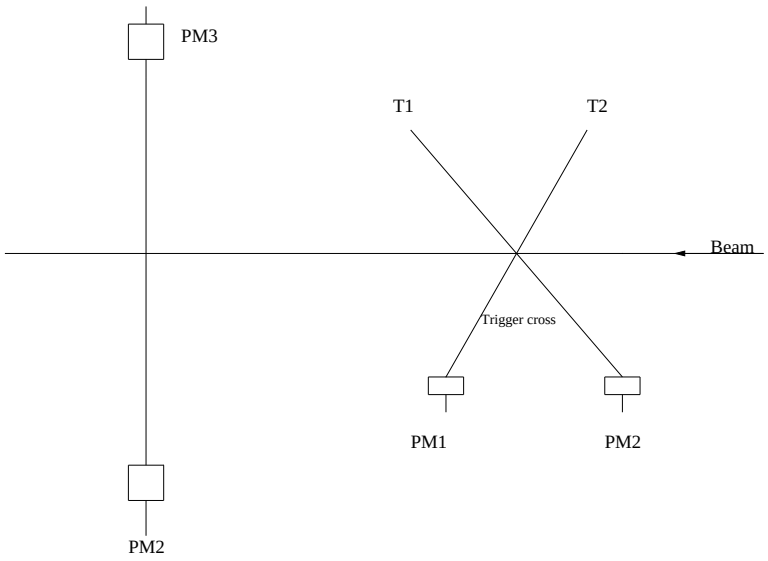

Figure 24: Schematic view of the test beam were done in Mainz

The trigger cross consisted of two scintillator strips of 0.6 cm width, one horizontal (T1) and one vertical (T2). T1 and T2 were connected by a silicon cookie to a phototube on one side. The tested scintillator was red out by phototubes XP2900 (PM3, PM4) via a cookie on both ends. In addition some of the scintillators were equipped with light guides on both sides. For all tests in Mainz we used the same phototubes.

The four PM signals PM1, PM2, PM3 and PM4 were split and fed in to CAMAC ADC's and NIM discriminators. The coincidence of the signals from T1 and T2 was used to generate a trigger gate, which provided the start signal for the TDC's and the gate for the ADC's. One output from each discriminator channel was delayed and fed into the stop of a TDC module.

We tested two types of material: Bicron 404 and 408, based on polyvinyltoluol, and Kuraray, based on polysteren.

5.1.2 Measurements

5.1.2.1 June test In June we used two different scintillator materials from Bicron: BC404 and BC408. For each material we tested two elements of differents sizes (20x21x1200 mm^3 and 20x25x1500 mm^3) as prototypes for H4HM and H5HM. They had a polished surface (diamond tool finished) provided by Bicron. For about ten different positions along the strips ADC and TDC spectra were taken with both PM's.

5.1.2.2 October test In October we tested two scintillators of 20x25x600 mm^3 size out of the Kuraray material, cut and polished in Warshaw. Both elements had light guides at both ends. We also used one element made of 20x25x1500 mm^3 Kuraray material polished by ourselves. In addition, one of the Bicron elements from the June beam time was remeasured.

5.1.2.3 December test In December we tested scintillators of 20x25x1500 mm^3 size for the H5HM produced in Warsaw out of Kuraray material called final 1, final 2 and final 3. The three scintillators had light guides. For comparison we remeasured one of the self polished Kuraray elements and one Bicron element. In addition to the standard electronics used in all test measurements we used the specially developed Orsay discriminators with meantimer.

5.1.3 Results

Figure 25 shows an example for an ADC a) and a TDC b) spectrum obtained with the scintillator final 1. Both spectra were taken 45 cm distance from the end of the scintillator, shown is the close PM spectrum. The time resolution of 212 ps was determined as the sigma of a gaussian fit to the TDC spectrum (see fig.25 b)). It still includes the 82.7 ps time resolution of the trigger cross, which implies a time resolution of 195 ps for a single PM of final 1.

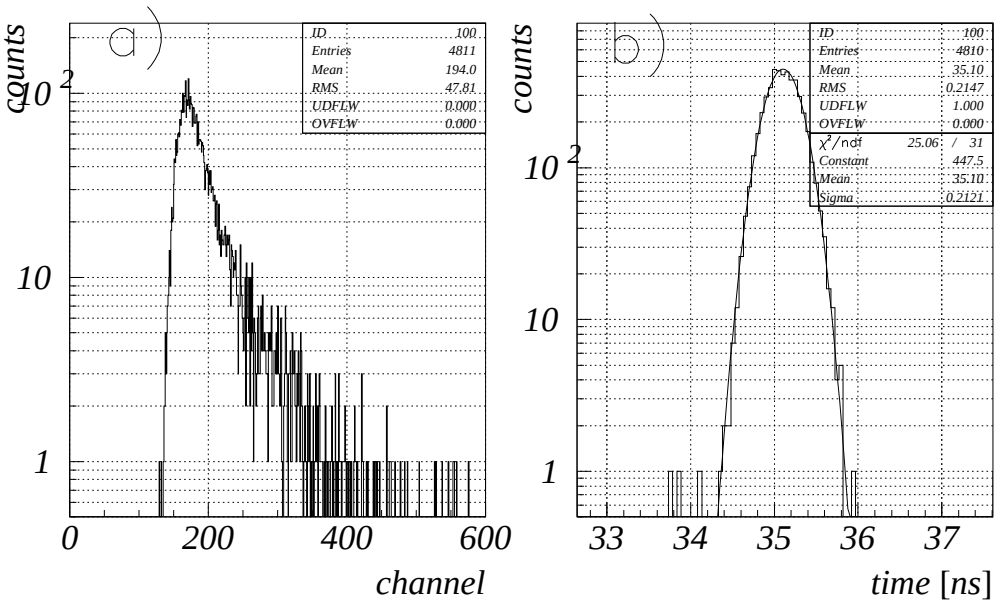

Figure 25: ADC and TDC spectrum for the scintillator final 1

Figure 26 a) shows the light attenuation curve for the same scintillator. Here the ADC pulse heights are plotted versus the position of the beam in the scintillator. The attenuation length of about 190 cm is the result of a fit with an exponential function. Figure 26 b) shows the position of the TDC stop peak for the both PM's and the calculated mean time $t_{mean} = (t_1 + t_2)/2$ versus the position of the beam in the scintillator. As can be seen the calculated mean time is constant to about 0.35 ns.

Table 10 summarizes the results for all the test measurements. To determine the final resolution of the scintillators we have to correct for the time resolution of the trigger cross. The time resolution of the trigger cross was 111.72 ps in June, 128.69 ps in October, 82.73 ps in December. The value PEAK is the calculated meantime, the error indicates the variation along the strip. SIGMA is the width of the meantime peak with the variation along the strip indicated as error. The time resolution of all scintillators is of the order of 160 ps and quite comparable with the Bicron scintillators some what better than the Kuraray ones. The same is true for the attenuation length.

But all scintillators fullfill the requirements of the COMPASS trigger. As the Bicron scintillators are more expensive we decided the use the Kuraray material for the prime hodoscopes.

In December we also did a comparison of the readout electronics. Figure 27 shows the positions of the TDC stop peak using Orsay CFD's and NIM CFD's versus the position of the beam in the scintillator together with the calculated meantime. In addition the value of the measured meantime with the Orsay meantimer is plotted. The three meantimes were constant to about 0.3 ns.

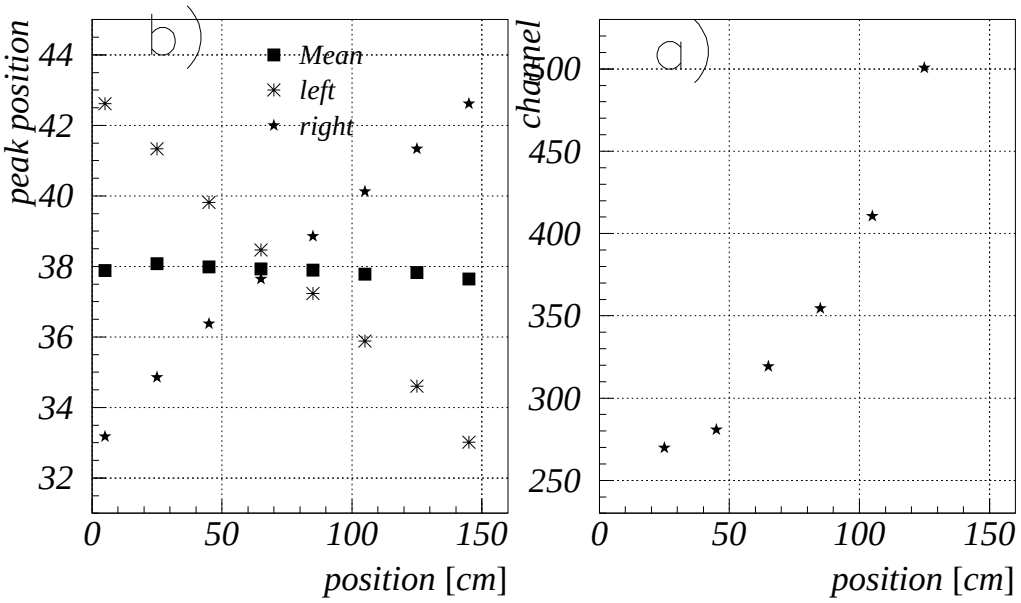

Figure 26: a) Attenuation curve and b) TDC stop peak position for the scintillator final 1

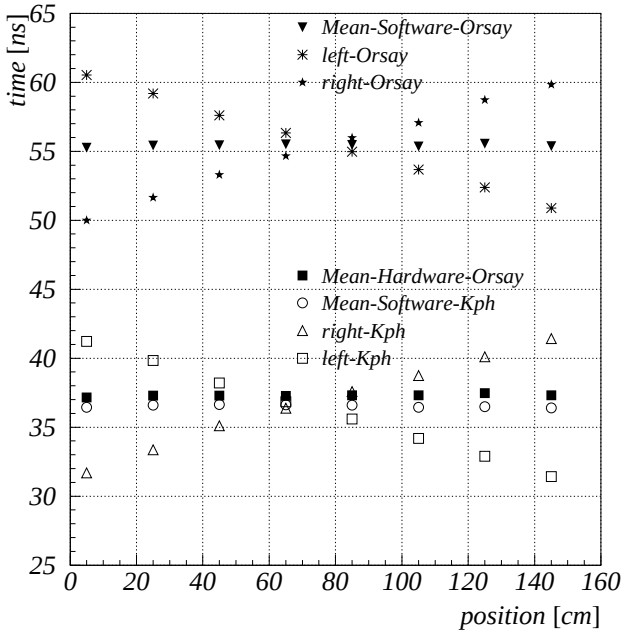

Figure 27: Comparison between the results obtained with NIM (Kph) and Orsay discriminators for the scintillator final 1

Date	Material	PEAK[ns]	SIGMA[ns]	Atten.[cm]		*Threshold [mV]*	
				left	right	left	right
June 99	Bicron Element 1	33.17 +-0.28	0.116 +-0.021	190.	193.	—	—
June 99	Bicron Element 2	38.39 +-0.09	0.115 +-0.015	212.	178.	—	—
October 99	Kuraray Element 1	17.88 +-0.37	0.201 +-0.021	108.	93.	-34	-28
October 99	Bicron Element 1	17.16 +-0.15	0.165 +-0.026	174.	175.	-34	-28
December 99	Kuraray Element 2	35.34 +-0.53	0.183 +-0.012	145.	160.	-50	-50
December 99	Bicron Element 2	35.16 +-0.47	0.132 +-0.03	182.	190.	-150	-150
December 99	Kuraray final 1 1350 V	37.21 +-0.37	0.166 +-0.031	169.	—	-100	-100
December 99	Kuraray final 1 1400 V	36.53 +-0.25	0.18 +-0.03	162.	194.	-100	-100
December 99	Kuraray final 1 1250 V	37.97 +-0.2	0.171 +-0.035	189.	190.	-100	-100
December 99	Kuraray final 2 1300 V	36.28 +-0.43	0.200 +-0.035	187.	238.	-50	-50
December 99	Kuraray final 3 1500 V	34.74 +-0.28	0.162 +-0.03	155.	133.	-50	-50

Table 10: The results for the measurements in Mainz

6 Muon Test Beam 1999

The M2 testbeam periods in July and September 1999 provided the first opportunity to test the performance of the chosen trigger hardware and to prove the trigger concept in an environment similar to the final one. For this purpose prototypes of all crucial parts of the trigger system were produced. Figure 28 and 29show a schematic view of the relevant hardware for the trigger test in the experimental area.

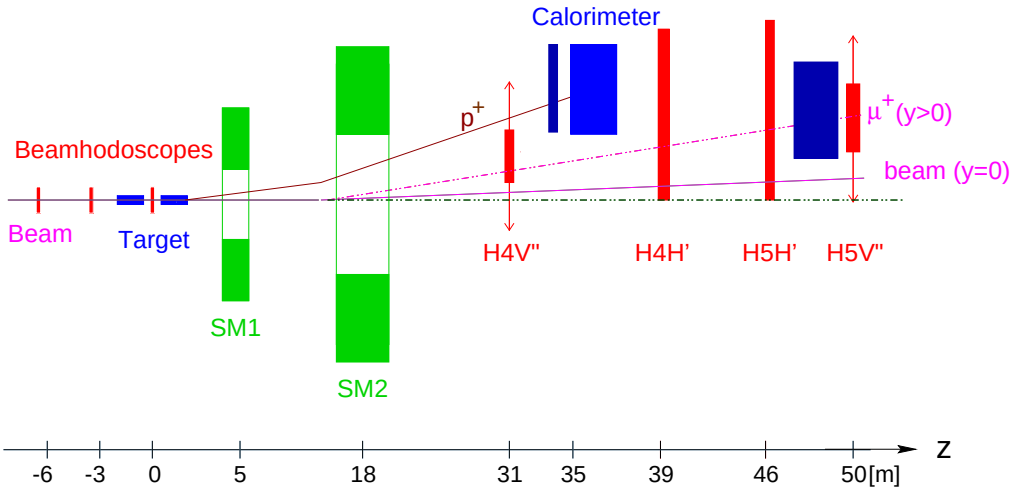

Figure 28: Schematic view of the testbeam

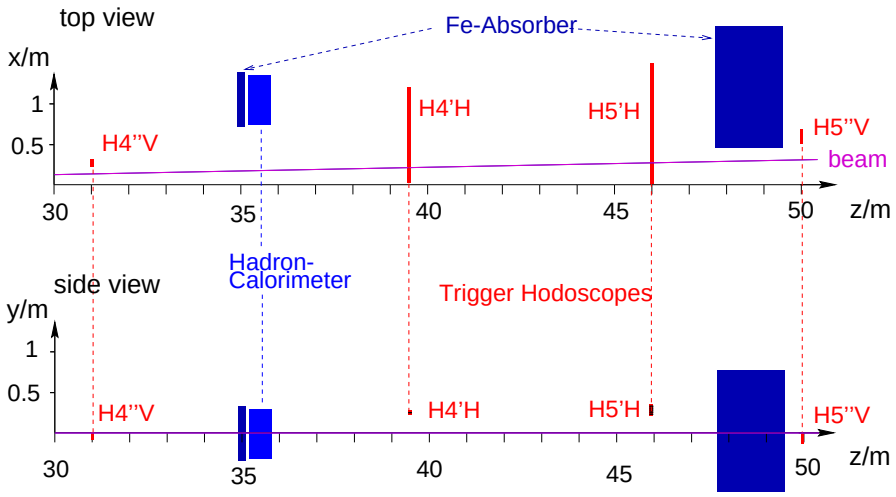

Figure 29: Position of the hodoscopes and the hadron calorimeter

Up to four small scintillator hodoscopes situated in the target region were used to measure the beamprofile. The two planes (horizontal and vertical) of one of these hodoscopes were also included in the trigger readout system to permit a beam definition in the analysis. Two rods polyethylene (3 cm diameter and 60cm long each) took the place of the final target giving a similar mass distribution. To allow a realistic test of the energy loss trigger concept as described in 2 both magnets were powered at nominal currents thus giving the full dispersion. The two double prime prototypes were located at their forseen positions and both were moveable over a wide range in the x–direction (indicated by the arrows in fig. 28). That way the prototype could not only cover the half acceptance of the final hodoscopes but even allow investigations of the undeflected beam. These hodoscopes are used to select scattering processes with a scattering angle $\theta < 5$mrad and an relative energy loss of the muon $y > 3$. In addition to this 'energy loss trigger system' a small part of the horizontal prime system, which accepts muons with 5mrad$< \theta <$ 15mrad, was prepared and tested. These partly equiped

hodoscopes could also be moved to cover the full acceptance. Sixteen hadron calorimeter modules delivered additional signals to study the cleaning effect of hadronic information on the trigger.

In addition to the detector prototypes plotted in fig.28 several new electronic modules were tested during the data taking, namely a prototype discriminator board with the 16 orsay discriminators, a complete matrix board and prototype of the calorimeter summation electronics.

The following subsections will deliver a more detailed description of the used hardware and summarize the most relevant results obtained during the test beam. A brief discussion about trigger properties will be given at the end of the description of each trigger system.

6.1 Beam properties

Horizontal intensity profiles of the muon beam were obtained by moving the hodoscopes H4VI and H5VI along the x–direction and counting the single rate of each element. Similarly, a vertical profile was measured by rotating H5VI by 90^o and moving it up and down.

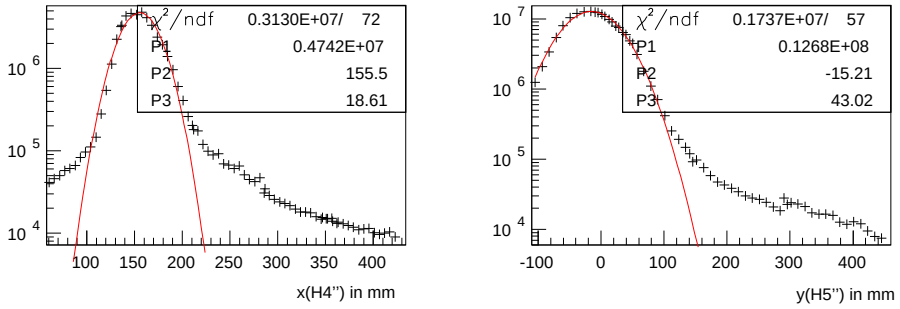

Figure 30: Measured beam profiles

As a result Fig. 30 shows a horizontal profil at $z = z(\text{H4VI}) = 31m$ and a vertical profile at $z = z(\text{H5VI}) = 50m$. For the divergence of the gaussian core of the beam typical values $\alpha_x = 0.65$mrad, $\alpha_y = 0.85$mrad were extracted. Approximately 5% of the beam intensity is located outside the 3σ region in non–gaussian tails (see Fig. 30).

6.2 The Double Prime System

6.2.1 The Hardware Setup

6.2.1.1 H4VI The H4VIprototype consisted of 16 channels, presenting a quarter of the final setup. BC404 sticks with the dimensions 205x10x6mm^3 were used as scintillators. A silicon cookie provided the light coupling to the R7400 HamamatsuHamamatsu Photonics Switzerland[8] tube. The optical contact was guaranteed by pressing the PM against the scintillator with a spring. The spring, the PM and the Mainz base were housed in an aluminum tube (20x1.5mm). Due the small effective width of the scintillators they were stackered in four rows. An inclination angle of 25° was chosen to optimize the timing between H4VIand H5VI.

6.2.1.2 H5VI Beside the inclination the design of the H5VIis quite similar to the one of H4VI. Its measures are just scaled to the different distance to the target and pivotal point. The 16 scintillators were 280mm long, 12mm broad and 20mm deep, they were also stackered in 4 rows. The philips tube XP2900/01 was used to read out H5VI.

6.2.1.3 Calorimeter For the tests of the summation electronic of the hadron calorimeters only a small part (4x4 cells) of this detector was equiped. The analog sums of each 4 of this cells were fed to ADCs which were included in the trigger readout. The sum of all 16 cells was given two a discriminator, whose outputs were used to feed a TDC and to enter the trigger as an additional condition, thus allowing an enrichment of 'hadronic' events in the data sample, which was, due to the small acceptance of the calorimeter, essential for studying the impact of calorimetric information on the trigger.

[8] http://www. hamamatsu.com

6.2.1.4 Trigger Electronics and Readout A schematic overview over the setup of the electronics and the data collection is shown in figure 31. First, the incoming analog signals were split, one branch going directly to standard CAMAC ADCs, the other fed into the discriminator board. The discriminator board 4.3.3 was a 6U VME carte with 16 orsay discriminator modules on it. Via the VME the threshold of each CFD could be adjusted by software. Two of the three possible outputs of the CFD board were used to deliver signals to a standard CAMAC TDC (via two level translaters) as well as directly to the matrix board. The 6U VME matrix board was equiped with two 16 channel delay chips (as described 4.5.34.5.2) and one matrix chip (c.f.4.5.2). Not only the delay and the pulse forming of the delay but also the matrix pattern could be easily changed via the PC. Using the fan out feature of one of the level translaters another copy of the logic signals were sent to CAMAC scalers.

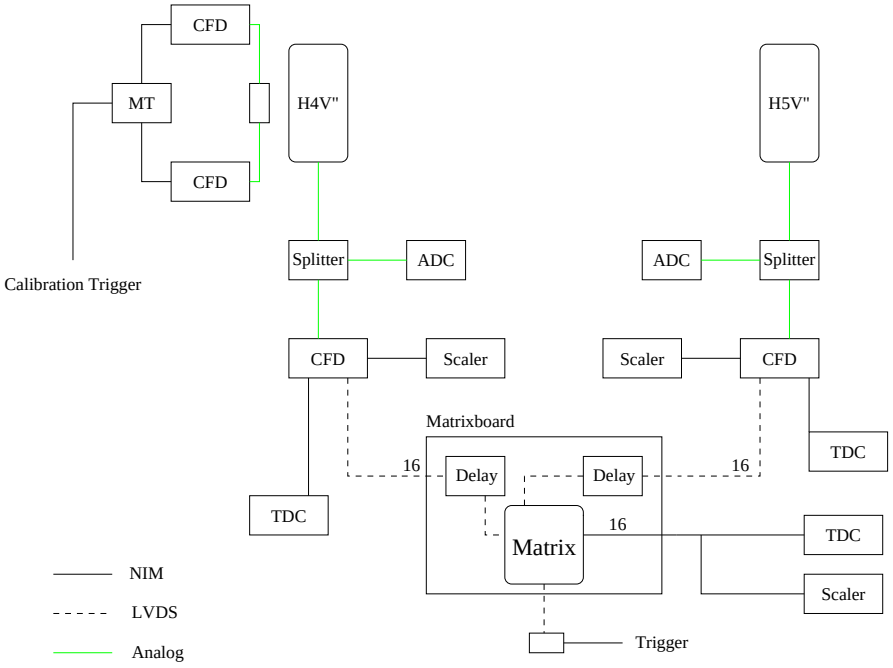

Figure 31: Schematic view of the testbeam electronics

The readout was done by a CAMAC–SCSI interface from Jorway. This CAMAC crate controller was adressed by a self made readout software via the SCSI branch. The trigger pulse and the busy signal were transported via the printer port of the PC. The former is causing an interrupt which starts the readout of the crate. The trigger was formed by NIM electronics providing several kind of triggers whereas the most widely used was the coincidence between the two total OR of H4VIand of H5VI.

6.2.2 Performance of the Hardware

6.2.2.1 Pulse Height To allow an effective rejection of the noise by the CFD without cutting out real signals a clear separation of both in terms of pulse height is needed. The two detectors with their short thick scintillators should not impose big problems in this issue. Nevertheless the weak amplification of the R7400 limits the reachable pulse height. Nevertheless, in the clean environment of the MAMIMAinzer MIcrotron[9] electron beam both detectors showed an excellent pulse noise ratio.

The investigation on the analog pulses with an oscilloscope already confirmed the expectations from the former tests: both hodoscopes –H4VIand H5VI– delivered pulse heights of 150mV and 500mV respectively at operating voltages below and around the typical voltage quoted in the literature, with an sufficient low noise level to allow threshholds of 30mV and 100mV. The ADC spectra – fitted with a Landau function – plotted in figure 32 verify this observations.

6.2.2.2 Rate Stability As a side effect of the frequent use of the hodoscopes for beam scans, the rate stability was investigated. From beam tests at MAMI the rate limit was known to be higher than 2MHz.

[9] http://www.kph.uni-mainz.de

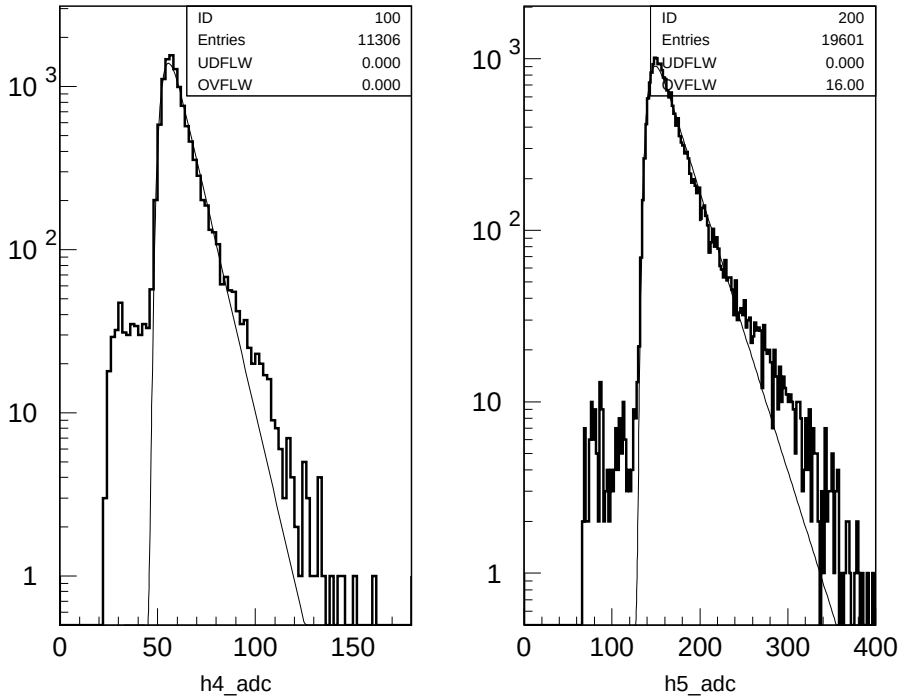

Figure 32: ADC spectra of H4VIand H5VI

By moving the hodoscopes in the beam center at nominal beam intensity of $2 \cdot 10^8 \mu/spill$ a single strip rates of $4 \cdot 10^6$ and $1.5 \cdot 10^6$ for H5VIand H4VIwere observed without any visible impact on the scaler spectra. The rates at the nominal position of these hodoscopes will – as expected – not pose any problem for the equipment.

6.2.2.3 Time Resolution The most critical parameter of this detector pair is the time resolution between both, since this resolution determines the minimal coincidence time ($\tau_m in = \pm\sigma_t$), i.e. to permit a coincidence time of 2ns a resolution better than 200ps must be achieved. According to the results from various tests at the electron beam, were single strip time resolutions below 100ps were achieved, one could expect the time resolution of the system to be below 140ps. However the situation in the muon beam is quite different than in the point like electron beam. In M2 the time difference between one element in H4VIand H5VIwas measured over the full length of the scintillator thus being sensitive to e.g. the correct choice of the inclination angle **??**.

Figure 33 shows the time difference between one element in H5VIand H4VI, without any additional cut. The well fitting gaussian curve has an sigma of 187ps, which lies below the desired value, proving that the full chain (Scintillator, PMT and CFD) is well designed for the demands.

6.2.2.4 Matrix Delay Curve After achieving the sufficient timing one expects to measure a delay curve with the desired width of 2ns. Taking advantage of the software controlled delay on the matrix board, the delay curve was done automaticaly. Figure 34 shows a typical curve, its width is indeed about 2ns.

6.2.2.5 Reliability During the whole test beam period none of the new equipment failed or showed any kind of abrasion. This gives a rather good impression on the reliabilty of the equipement.

6.3 The Prime System

6.3.1 The Hardware setup

The hardware of the prototype prime system consisted out of two hodoscopes planes H4HM and H5HM. H4HM was located at position 39.6 m and H5HM at position 46 m. Both, H4HM and H5HM, were positioned behind a 160 cm thick concrete absorber. Both hodoscopes were mounted 17.2 cm above respectively below the muon beam and could be moved in steps of 4 cm respectively 14.4 cm in the vertical direction.

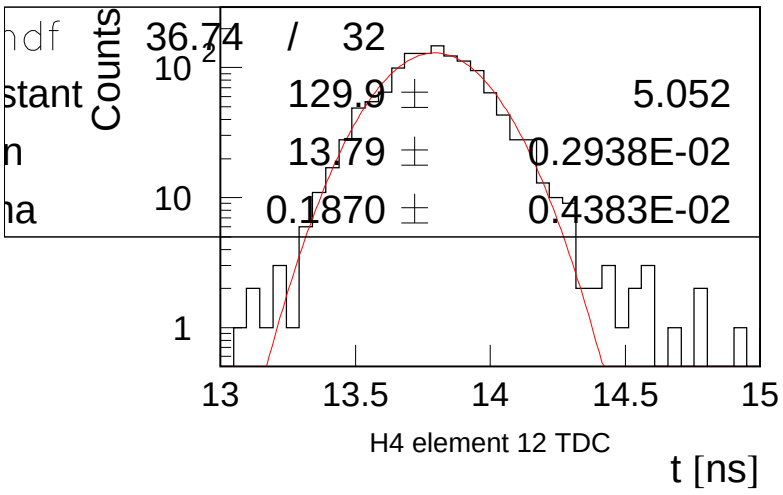

Figure 33: Timeresolution of the double prime system with orsay CFD.

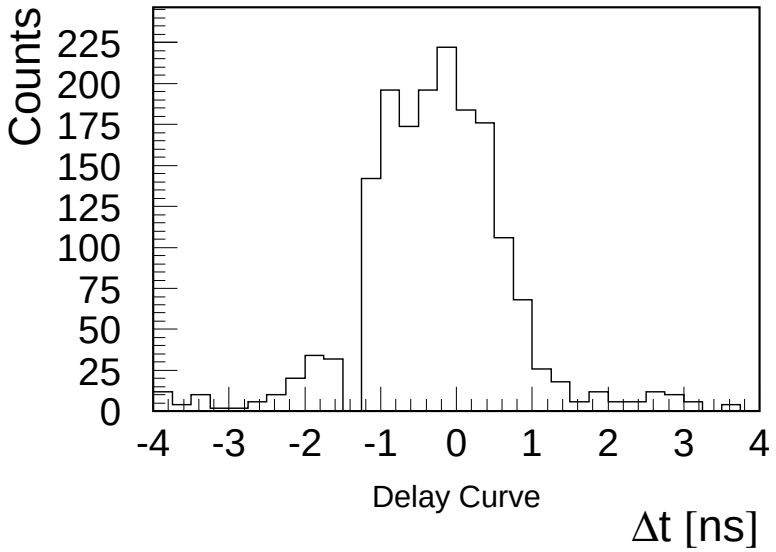

Figure 34: One coincidence curve of the Matrix.

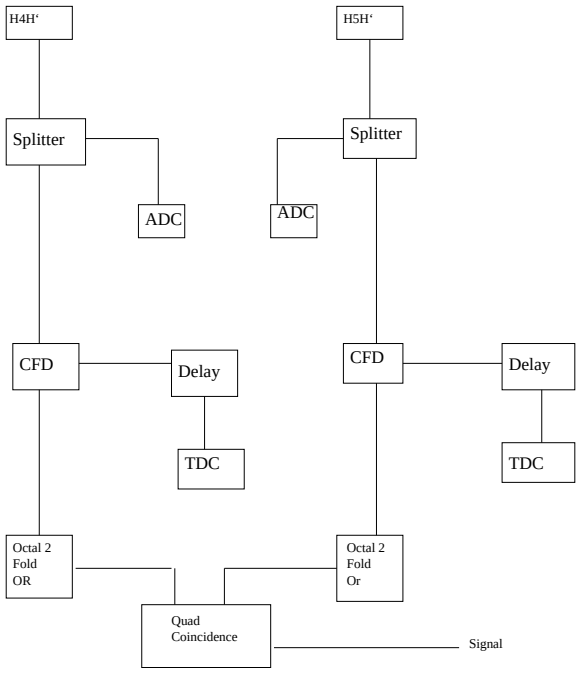

Figure 35: Schematic view of the test beam electronics for the prime system.

6.3.1.1 H4HM The H4HM prototype consisted out of two horizontal strips. They were made out of two differents materials: Bicron 404 and Bicron 408. Both elements were delivered with diamond tool finished surface and were wrapped in aluminium foil. They had dimensions of 1200x20x21 mm^3. A silicon cookie provided the light coupling to the Philips tubes XP2900, mounted at both ends. The optical contact was guaranteed by pressing the photomultiplier against the scintillator with a spring. The spring, the PM and the specialley designed Mainz base were housed in an aluminum tube. There was an overlap of 1 mm between neighbouring strips.

6.3.1.2 H5HM The H5HM prototype consisted out of six horizontal strips from three differents materials: 1 element of Bicron 404 scintillator, 1 element of Bicron 408 scintillator and 4 elements of Kuraray scintillator. The four elements from Kuraray material were cut at CERN and polished by ourselves. All strips were 1.50 m long, 20 mm deep and 25 mm wide. The scintillators were wrapped in aluminium foil. The PM's, cookies and bases were the same as for H4HM. There was an overlap of 1 mm between neighbouring strips.

6.3.1.3 Trigger electronics and readout A schematic overview over the setup of the electronics is shown in figure 35. The anode signals from the PMs were split into two. One of them was used for charge measurement and connected to a LE CROY 2249A ADC. The other signal was used for time measurements. This signal was discriminated using a quad discriminator and then connected to a LE CROY 2228A TDC with a resolution of 50 ps/channel. The readout was done by a CAMAC SCSI interface from Jorway. A coincidence signal was obtained from an AND between the signal from a logical OR of all outputs on the jura side of the hodoscope H4HM and the signal from a logical OR of all outputs on the jura side of the hodoscope H5HM.

6.3.1.4 Measurement of halo profiles Halo profiles were obtained by moving H4HM and H5HM along the z-direction and counting the single rates of each element. The results for H5HM are shown in figure 36. The profile is asymmetric with the rates between 50 and 450 kHz for positions below the beam and between 50 and 1150 kHz for positions above the beam.

6.4 Trigger studies with muon beam

Apart from testing recently developed electronic components one goal of the beam times in July and September 99 was – as mentioned before – to investigate experimentally the purity of the trigger scheme described in 2. These studies focussed onto the investigation of effects from the target. Particularly due to the renunciation of

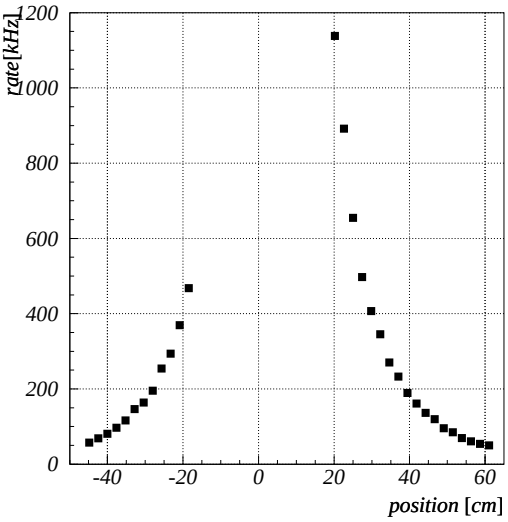

Figure 36: Halo profile of the muon beam measured with H5HM.

a system of veto detectors to reject halo muons it had to be proved that correlated hits in 2 hodoscope planes and a hadron detection in the hadron calorimeter are sufficient to make a trigger decision.

Figure 28 shows a schematic overview of the experimental setup that was used to investigate two critical trigger components:

1. Selection of quasireal scattering processes with scattering angles Θ <5 mrad and relative energy losses y >0.3 using the two hodoscopes H4VI and H5VI.
2. Selection of muons with Q^2 > 0.5 GeV^2/c^2 (Θ >15 mrad) using the horizontal H4HM and H5HM hodoscopes.

Detailed descriptions of these hodoscopes are given in chapter 6.2.1 and 6.3.1.

6.4.1 Trigger on quasireal photon events

For the data that are discussed in this section the hodoscopes H4VI und H5VI covered the range 22.3cm< x_1<30.9cm and 49.2cm<x_2<66.8cm where $x_1 = x$(H4VI) and $x_2 = x$(H5VI) are the horizontal hit positions in both hodoscope planes. This acceptance is located outside the three sigma region of the gaussian core of the beam.

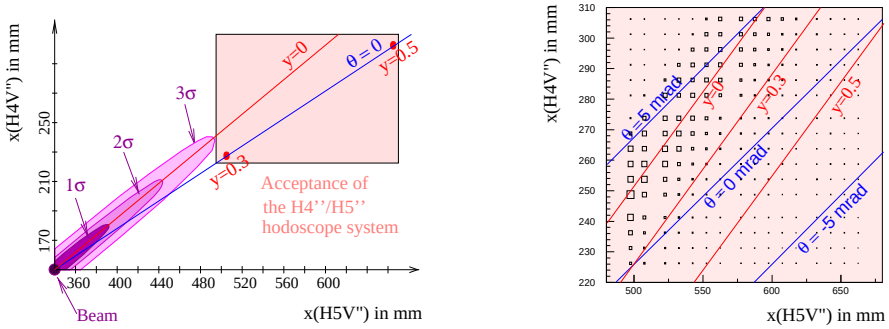

Figure 37: Correlation of hit positions $x_1 = x$(H4VI) and $x_2 = x$(H5VI) schematically and with real data.

Figure 37 shows symbolically the correlation between x_1 and x_2 for muon tracks. As outlined in section 2.1 the relativ energy loss y and the scattering angle Θ for these tracks can be calucated from the pair (x_1, x_2). As an illustration some lines with constant values for y and Θ are plotted in Figure 37.

The right hand of Fig. 37 shows the acceptance of the hodoscopes populated with real data triggered by coincident hits in the two hodoscopes alone. No hadron detection was demanded. A strong correlation along the line $y = 0$ =const can be observed. These events with no energy loss originate from the tail of the beam and no target effect is expected here. The coincidence matrices (see sec. 4.4) will later allow to reject this event class in the trigger decision.
Muons leaving the target e.g. with scattering angle $\Theta = 0$ and a finite energy loss are correlated along the line $\Theta = 0$ =const. A negative muon scattering angle indicates that the direction of the emission in the target was opposite to the deflection in the magnetic field. On the left side of Fig. 38 the shape of the recontructed y–distributions with and without a target are compared. Only a small difference can be observed in data samples recorded under these tigger conditions. The numbers of entries in the spectra have been normalised via a current signal of a ionisation chamber in the muon beam to the number of 10^8 incident muons. The

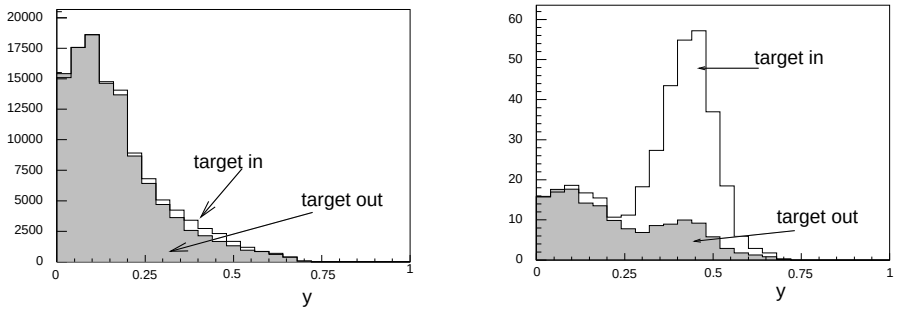

Figure 38: Distributions of the relative energy loss y. The data shown on the left hand side were selected by coincident hits in both hodoscopes alone. On the right hand side in addition a coincident hadron detection was demanded in the trigger decision.

picture changes when in addition a hadron detection is demanded. The shape of the y–distribution in Fig. 38 is modified and a clear target effect arises. The TDC information of the hadron calorimeter that was available

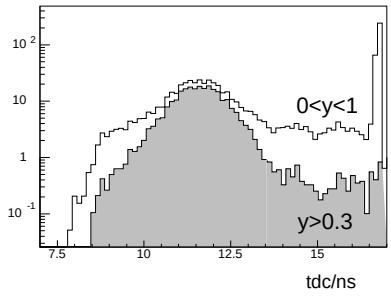

Figure 39: TDC information of the hadron calorimeter. The signal to background ratio is in total 7:1 but increases to 23:1 for events with $y > 0.3$.

during these test runs is plotted in Fig. 39.
To investigate the relative importance of events where the hit in one of the hodoscopes originated from other particles instead of the muon itself, a hadron or a second muon for instance, a small scintillation detector was added between H4VI and H5VI. For a muon track penetrating both hodoscopes one can predict whether there is a hit in this additional detector or not. At the beam intensity of $I_\mu = 10^8 \mu/spill$ and complete trigger conditions (H4VI $\wedge$ H5VI $\wedge$ hadron detection) 96% of all events do fulfill this prediction.

6.4.2 Trigger on events from deep inelastic scattering

Figure 40 shows schematically the hodoscope setup used to test the trigger for events with $\Theta \approx 5$mrad.

The vertical positions of a muon track $y_1 = y(\text{H4M})$ and $y_2 = y(\text{H5M})$ are given by. $y_1 = y_0 + \Theta_y \cdot z_1$ and $y_2 = y_0 + \Theta_y \cdot z_2$. Here y_0 is the vertical offset of the track at target position ($z = 0$). The horizontal

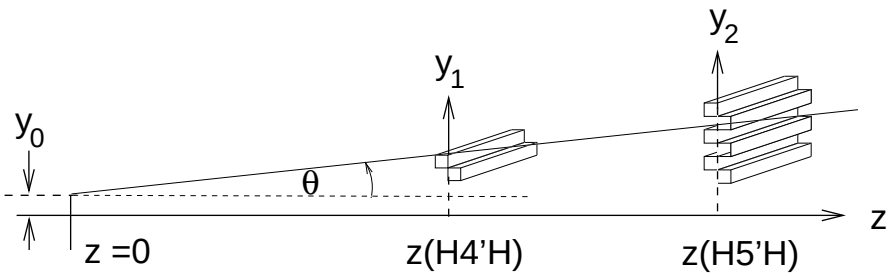

Figure 40: Setup of the H4HM and H5HM test hodoscopes

hit positions can be calculated via the different propagation time of the scintillation light to the phototubes at both sides of the detector.

7 Trigger test procedures

The philosophy of the trigger of the muon scattering experiment of COMPASS has been described in chapter **??**, while its realisation in terms of electronic components can be found in section 4. The two most important parameters for its performance are

$$\text{the trigger efficiency} = \frac{\text{selected number of good candidates}}{\text{true number of good candidates}}$$

$$\text{the trigger purity} = \frac{\text{selected number of good candidates}}{\text{selected number of candidates}}$$

While a high purity minimizes the flow of unwanted data and thus the dead time losses a high trigger efficiency maximizes the statistical precision of the experiment at a given luminosity or vice versa. For asymmetry measurements as foreseen in COMPASS the trigger efficiency must not fluctuate in a correlated way with the spin reversal. Of course a trigger efficiency constant in time is generally preferable. (NB: A fluctuating trigger purity of course also (indirectly) influences the net trigger efficiency due to varying dead time losses). For absolute cross section measurements as may become desirable in the COMPASS experiment the trigger efficiency has to be known absolutely and therefore experimentally determined and continuously monitored. In a strict sense this can only be done through introduction of an additional low bias trigger system to provide events which can be checked offline for their justification as good candidates. The fraction of those for which a trigger signal had been generated by the trigger system at run time determines the trigger efficiency. Unfortunately the step from the devised COMPASS trigger system with two hodoscope planes down to one plane for a low bias system would dilute the rate of good candidates so much that the obtained statistical precision in the trigger efficiency will be rather poor for acceptable dead time losses. The only way to monitor the trigger efficiency and the system performance in general therefore consists in splitting the chain of signal processing devices (as are hodoscopes, discriminators, matrices and additional coincidence logic) into sub chains which can be checked and monitored separately in special procedures.

7.1 Hodoscope elements

A comprehensive way to monitor the performance of the elements (light collection, PMT, cable connectors etc.) can in principle be provided by equipping each channel with an ADC to obtain pulse height spectra of either mips or other reference particles from a radioactive source. This, however, implies additional effort and cost. As a cheaper solution a certain number of spills could be used during which the discriminator thresholds could be stepped through and the corresponding output rates be registered by the standard scalers connected to the discriminators (fig. 9. In this way a single channel analyser is emulated and an integrated pulse height spectrum is obtained. Technically this requires a fast step through procedure and, of course, is at the expense of spills which are then lost for physical data. On the other hand the investment is limited to the sector of software and the scheme could be run at a relatively early stage of the experiment. For the measurements of asymmetries this procedure is considered sufficient and appropriate.

7.2 Discriminators

A properly working discriminator is characterized by its function to generate a digital output pulse on the ocurrence of any analog input signal the pulse height of which exceeds some preset threshold and to maintain a strict correlation in time between that and the output pulse (constant propagation delay). The verification of proper threshold setting is implicitly included in the previously described single channel analyser mode but cannot be uniquely separated from the hodoscope performance without additional investigation by hand. The digital signal path can be checked by feeding in or generating (digital) test pulses which then have to arise as entries in the TDC's at a well defined time with respect to a reference start/stop pulse (extra trigger e.g.). A strict check of the time correlation between the output and the *analog* input signals which is actually relevant for the physical data requires additional equipment and is presently not foreseen.

7.3 Coincidence Matrices

These devices are to detect coincidences of signals of correlated hodoscope strips with high efficiency at the shortest possible coincidence overlap time (2 nsec typ.). To this aim both, the relative time of the input pulses as delivered by the discriminators at arrival in the respective internal logical AND-gates as well as their width can be set and modified by special delay chips in the matrix modules (see chapter **??**). By software controlled stepping of the relative signal delay a delay curve of the rate of matrix output pulses can be taken. For the

normal running the signal delay can thus be set deliberately e.g. in a symmetric way for minimizing the necessary time width of the signals (and thus the rate of accidental coincidences) or in an asymmetric way to tie the trigger timing to a predefined hodoscope plane. Again it is important to note that this procedure relies on the relative stability of the propagation delays between the analog and digital inputs of discriminators, resp. and the digital outputs which are fixed to some nominal values by construction and checked during the release procedure of the modules. A later deviation of the propagation delay for the analog signals due to malfunction will only be become obvious as acceptance holes in the physical data. The described procedure has already to be used during the set up of the trigger system and will therefore be available from the very beginning of data taking.

7.4 Hadron Calorimeters

Here the crucial performance parameters to be monitored are the stability and uniformity of the effective calorimeter thresholds as well as the propagation delays between the incident hadron and the generated output signals for the full amount of modules. The most comprehensive way to monitor these performance characteristics makes use of a triggered exposure of the calorimeter by, say, mips. Presently, however, no trigger device of the required area is at our disposal and alternatives have to be resorted to. Instead, all calorimeter channels could be equipped with a second set of discriminators continuously operated at thresholds significantly below 1 mip. Alternatively, the thresholds of the running discriminators could be accordingly set for extra spills at the expense of running time. In either way the position of the 1 mip peak in the pulse height spectra could be monitored. This scheme does of course not provide a check of the relative timing of the individual calorimeter modules with respect to the incident particle nor does it monitor the proper time correlation of the calorimeter signal relative to the signal derived from the scattered muon with which it is to be checked for coincidence. As far as I can see the only way to provide that is to regularly run for intermittent periods (possibly with lower luminosity) with the coincidence overlap time between calorimeters and muon system wide open and to verify that the time distributions of the calorimeter signals from true coincidences as recorded by the TDC's are not cut off by the actual run settings.

8 Online programs

In order to control the various parts of the trigger system a system of online software is needed, that needs to fit into the general online — or slow control — scheme of the COMPASS experiment. The general slow control for COMPASS is developed in close collaboration with IT/CO[10]. There a commercial SCADA[11] system is used, which will provide a user interface, data storage and alarm handling facility. The interfacing of the trigger online software to that general scheme is done using a software tool from the Delphi collaboration which is called DIM[12], for Distributed Information Management system.

8.1 Program structure

Figure 41 shows an overview over the software structure.

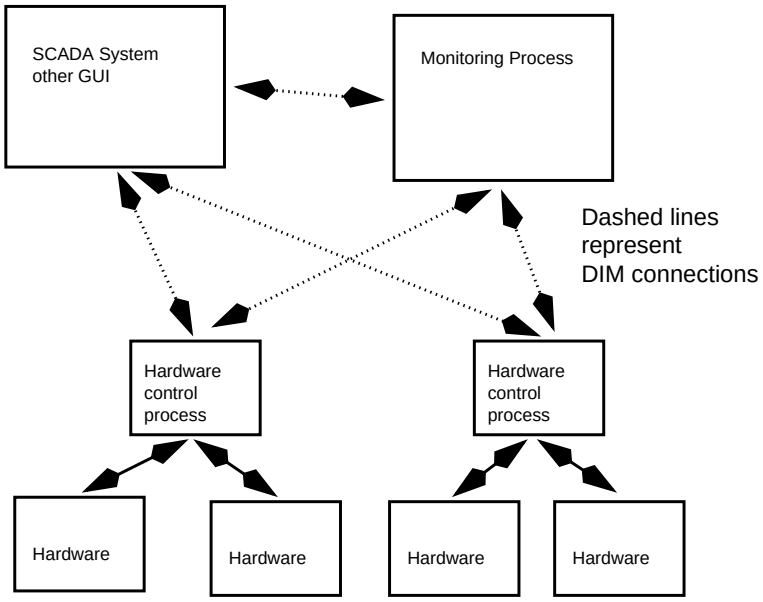

Figure 41: Structure of the online software

In bottom-up order it is as follows: The hardware is controlled by hardware control processes, each of which controls several instances of the same hardware, for example one control process for all the discriminator cards in one VME-Crate. These hardware control processes are tied to specific machines, because they need the direct contact to their boards, thus they run on the VME CPUs.

On the top of this hierarchy sits the SCADA system, which provides the user interface to the control processes.

Rather aside from the SCADA we find monitoring processes, which do periodic checks for the data consistency, doing tasks as defined in section 7. If a monitoring task needs to set values on the hardware, it tells the hardware control process via it's DIM interface to do so.

This architecture allows to keep the different tasks well separated, making changes to the single components easier.

8.2 DIM interface

The DIM interface allows to "publish" some values, which may then be read or written using the DIM mechanisms incorporated in the DIM library. Such values are for example the discriminator thresholds, high voltages or enable/disable patterns.

The DIM interface can then be used to couple the trigger software to the general SCADA system, but also too hook up a local user interface based on TCL/TK[13] or something else, a useful possibility to test and debug

[10] http://itcowww.cern.ch/compass_dcs/
[11] Supervisory Control And Data Acquisition
[12] http://delonline.cern.ch/d$onl/communications/dim/doc/www/dim.html
[13] http://www.scriptics.com/

the software in the lab independent of the expensive SCADA license, but still having only one version of the online software.

8.3 General features of the online software

8.4 Hardware control processes

The online software that is used to control VME boards must be able to communicate with these boards, so a link to the VME must be provided. For flexibility in this respect the software should try to encapsulate the VME accesses in a clean interface, so that it becomes easier to use different VME access hardware. The standard VME hardware, however, will consist of VME CPUs running Linux, and equipped with a Tundra Universe PCI to VME interface chip [8]. The Linux driver[14] for this chip was written some time before, but is continually developed to fit to the emerging newer kernels as well as added requirements on the functionality.

Since the VME interfaces of both the discriminator boards and the matrix boards are built with FPGAs, the online software provides a means to load these VME-Interfaces under software control, using the built-in configuration interfaces of the boards. This feature is now well tested in the 1999 beam time and the lab and provides no problems.

Also the identification of the VME boards is possible in software, because the addresses of the boards will be given in an unique pattern, so that with a database lookup, the actual implementation of which is still to be defined, from the base address of a board, which can be found out by scanning the address range of the VMEBus, the identification of the module is possible.

8.4.1 Discriminator control software

The discriminator control software will control all the software settable parameters of the discriminators, which are (see section 4.3.2):

- Thresholds of all individual channels
- Enable/Inhibit of all individual channels
- Meantimer threshold voltage for all individual mean timers
- Test pulse generation

8.4.2 Matrix control software

The matrix control software will control all the software settable parameters of the matrices, which are (see section **??**):

- Delay and Pulse widths of all input and output channels
- Matrix pattern
- Boundary scan on delay and matrix chips
- matrix overlap mode, see 4.5.2
- delay chip operation mode, see 4.5.3

8.4.3 HV control

High voltage is delivered by two different systems, CAEN SY527 and LeCroy 1440. The CAEN is the standard solulution within COMPASS, the LeCroy a legacy ststem from Bonn and Mainz, which will be used at least in the commisioning run in 2000. For the CAEN we expect that the control is done by IT/CO or someone else, for the LeCroy 1440 we will use a DIM enhanced version of the software used in the 1999 test beams.

8.4.4 Position monitoring

The position monitoring and control of the hodoscopes, see section **??**, has to be done by a dedicated software task, which feeds the position measurements to the slow control and takes commands to move to a specified position. Because here the hardware is not yet defined the software also is somewhat open.

[14] http://lisa2.physik.uni-bonn.de/ hannappe/software/index.html

8.5 Higher level processes

The higher software levels are again split into several processes wich may communicate with each other, the user or the hardware control processes. In the high level processes the algorithms for testing and setup, as described in section 7 are brought to live.

For firing them up via the general slow control system a process has to run permanently, so that a command sent via DIM can be employed to start a program that does the task required.

Also we need in this context some interlocking with the DAQ, because some test algorithms require settings of the hardware that are not compatible with standard data taking. This mechanism is still to be defined.

Also a decision has to be made if the lower levels of some of the algorithms are to be pushed into standalone programs, for example the taking of data for a delay curve of the matrices, so that manual inspection of the data, and probably also the debugging becomes easier.

8.5.1 Delay curve measurements

Measuring delay curves is a task which does interfere with normal data taking, because the timing and efficiency of the trigger is destroyed. On one matrix it is possible to step the delay values of one direction, either row or column, in parallel, if just one or channel on the other direction or in case of the columns a one-to-one pattern in the matrix is enabled. Thus the 32 channels of a matrix can be checked in one go, taking 32 steps, because of the 5 bit resolution of the delay chips[15]. If one does not want to waste 32 spills (almost 8 minutes), it is necessary to have several delay settings in one spill, if the statistical precision allows this for outlying channels.

Delay curves present a special problem concerning readout: If one uses only TDCs to register the signals form the matrix rows a trigger is needed to record events, but that trigger may not come if the timing is to far off the normal value. The better solution is to use scalers for the matrix output, thus being insensitive to the trigger.

8.5.2 Threshold scans

Threshold scans conflict just as bad as delay curves with the data taking. Again the 256 possible threshold values require more than one step per spill or a decrease in resolution. On the other hand all channels of the complete system can be verified at once, with a slight inconvenience in the case of double sided counters. There one would need scalers for both ends of the counter in order to avoid having to scan the two ends independently.

8.5.3 Position scans

The last conflicting kind of scan is the position scan which is employed to measure beam profiles and ensure alignment. Of course the normal data taking cannot take place with the trigger hodoscopes not in their correct positions.

Due to the relation between hodoscope size and maximum displacement only a few (about 4) positions have to be taken to scan the whole accessible range of the beam. With the coincidence matrices wide open the trigger is not a problem in such a scan, allowing even event by event data taking and thus even measuring angular distributions.

8.5.4 Electrical checks

The purely electrical checks can be done during normal data taking, using either special calibration triggers if test pulses are used or during the inter-spill time.

In inter-spill time it is also possible to do some checks on the chips using the built in boundary scan.

[15] In a future Version of the delay chip that will be increased to 7 or 8 bits, increasing the number of steps by a factor of four or eight!

References

[1] AN-971: An Overview of LVDS Technology[16] National Semiconductor application note

[2] DS90C032 data sheet[17], National Semiconductor

[3] MC10124 data sheet[18], Motorola Semiconductors

[4] 0.8 μm CMOS Process Technology[19], Austria Mikro Systeme International AG, Schloss Premstätten A-8141 Unterpremstätten, Austria

[5] XC3000 FPGA Family data book[20] Xilinx, Inc. 2100 Logic Drive San Jose, CA 95124-3400

[6] CATCH documentation by the Freiburg group[21]

[7] F1 TDC Asic by the Freiburg group[22]

[8] Tundra Universe CA91C142 PCI/VME interface[23], Tundra Semiconductor Corporation Kanata, Ontario, Canada

[9] BC 404 data sheet[24], Bicron Corporation, 12345 Kinsman Road, Newburry, Ohio 44065-9677

[16] http://www.national.com/an/AN/AN-971.pdf
[17] http://www.national.com/pf/DS/DS90C032.html
[18] http://scgproducts.motorola.com/ProdSum.asp?base=MC10124
[19] http://www.amsint.com/products/technology/index_08.html
[20] http://www.xilinx.com/apps/3000.htm
[21] http://hpfr02.physik.uni-freiburg.de/compass/catch.html
[22] http://hpfr02.physik.uni-freiburg.de/compass/f1.html
[23] http://www.tundra.com/content_prod.cfm?tree_id=100361
[24] http://www.bicron.com/bc404.htm